Looking for $B \to X_s \ell^+ \ell^-$ in a nonminimal universal extra dimensional model

Avirup Shaw*

Theoretical Physics, Physical Research Laboratory, Ahmedabad 380009, India

(Received 3 April 2019; published 25 June 2019)

Nonvanishing boundary localized terms significantly modify the mass spectrum and various interactions among the Kaluza-Klein excited states of the five-dimensional universal extra dimensional scenario. In this scenario, we compute the contributions of Kaluza-Klein excitations of gauge bosons and third-generation quarks for the decay process $B \to X_s \ell^+ \ell^-$, incorporating next-to-leading-order QCD corrections. We estimate the branching ratio as well as the forward-backward asymmetry associated with this decay process. Considering the constraints from some other $b \to s$ observables and electroweak precision data, we show that a significant amount of the parameter space of this scenario has been able to explain the observed experimental data for this decay process. From our analysis, we put a lower limit on the size of the extra dimension by comparing our theoretical prediction for the branching ratio with the corresponding experimental data. Depending on the values of free parameters of the present scenario, the lower limit on the inverse of the radius of compactification (R^{-1}) can be as high as ≥ 760 GeV. Even this value could be slightly higher if we project the upcoming measurement by the Belle II experiment. Unfortunately, the forward-backward asymmetry of this decay process would not provide any significant limit on R^{-1} in the present model.

DOI: 10.1103/PhysRevD.99.115030

I. INTRODUCTION

Confirmation of the Standard Model (SM) of particle physics has *almost* been completed by the discovery of the Higgs boson at the Large Hadron Collider (LHC) [1,2]. However, the SM scenario is not the ultimate one, because there exist experimental data in various directions, such as massive neutrinos, the dark matter (DM) enigma, observed baryon asymmetry, etc., that cannot be addressed within the SM. This, in turn, ensures that new physics (NP) is indeed a reality of nature. Moreover, experimental data for several flavor physics observables (especially B physics) show significant deviation from the corresponding SM expectations. For example, B-physics experiments at LHCb, Belle, and *BABAR* have pointed at intriguing lepton-flavor-universality-violating (LFUV) effects for both the charge current ($\mathcal{R}_{D^{(*)}}$ [3] and $\mathcal{R}_{J/\psi}$ [4]) and the flavor-changing neutral current (FCNC) ($\mathcal{R}_K$ [5] and $\mathcal{R}_{K^*}$ [6]) processes. In the latter case, the involved processes are described at the quark level by the transition $b \to s\ell^+\ell^-$ (where $\ell \equiv e$, the electron, or μ, the muon), which is highly suppressed in the SM. Therefore, even for small deviations between the SM prediction and experimental data, these types of observables have always been instrumental in probing the favorability of the various NP models that exist in the literature. Apart from these, there exist several B-physics observables which could also be used for the detection of NP scenarios.

Following the above argument in the current article, we will calculate an inclusive decay mode $B \to X_s \ell^+ \ell^-$ in a NP scenario: namely, the nonminimal universal extra dimensional (nmUED) model.[1] This inclusive decay mode $B \to X_s \ell^+ \ell^-$ has been considered as one of the harbingers for the detection of NP scenarios. The reason is that this decay mode is one of the most significant and relatively clean decay modes. $B \to X_s \ell^+ \ell^-$ decay is significant in the sense that this decay mode not only helps in the detection of NP scenarios but also presents a more complex test of the SM. For example, in comparison with the $B \to X_s \gamma$ decay, different contributions add to the inclusive $B \to X_s \ell^+ \ell^-$ decay. Moreover, it is particularly attractive because, as a three-body decay process it also offers more kinematic observables such as the invariant dilepton mass spectrum and the forward-backward asymmetry [10,11]. At the quark

*avirup.cu@gmail.com

[1] In this model, we have already calculated several B-physics observables—for example, the branching fractions of some rare decay processes, e.g., $B_s \to \mu^+\mu^-$ [7], $B \to X_s\gamma$ [8], and $\mathcal{R}_{D^{(*)}}$ anomalies [9].

level, this process is also governed by the $b \to s\ell^+\ell^-$ transition. The effective Hamiltonian of this decay process is characterized by three different Wilson coefficients (WCs): C_7, C_9, and C_{10}. Among these WCs, C_{10} and C_7 for the nmUED model have already been calculated in our previous studies [7] and [8], respectively. Consequently, calculation of the WC C_9 using relevant one-loop Feynman diagrams in the context of the nmUED model is one of the primary tasks of this article. The full calculational details of the WC C_9 have been given in Sec. III. To the best of our knowledge, this is to be the first article where we will show the calculation of the WC C_9 in the context of the nmUED model in detail. Finally, with these different WCs (C_7, C_9, and C_{10}), we compute the coefficients of electroweak dipole operators for the photon and gluon for the first time in the nmUED scenario. Eventually, we can readily calculate the decay amplitude for this process, $B \to X_s\ell^+\ell^-$, in the nmUED scenario.

In most cases, the experimental data for several observables for the decay mode $B \to X_s\ell^+\ell^-$ have been more explored for two regions[2] of the dilepton invariant mass-squared q^2 ($\equiv (p_{\ell^+} + p_{\ell^-})^2$ spectrum. In these two regions, the experimental data of the branching ratio (Br) are given by the *BABAR* Collaboration[3] [14]:

$$\begin{aligned}
&\mathrm{Br}(B \to X_s\ell^+\ell^-)^{\mathrm{exp}}_{q^2\in[1,6]\ \mathrm{GeV}^2} \\
&\quad = (1.60^{+0.41+0.17}_{-0.39-0.13} \pm 0.18) \times 10^{-6}, \\
&\mathrm{Br}(B \to X_s\ell^+\ell^-)^{\mathrm{exp}}_{q^2\in[14.4,25]\ \mathrm{GeV}^2} \\
&\quad = (0.57^{+0.16+0.03}_{-0.15-0.02} \pm 0.00) \times 10^{-6}, (\ell = e, \mu). \quad (1)
\end{aligned}$$

The SM predictions for the above quantities are [15]

$$\begin{aligned}
&\mathrm{Br}(B \to X_s\ell^+\ell^-)^{\mathrm{SM}}_{q^2\in[1,6]\ \mathrm{GeV}^2} = (1.62 \pm 0.09) \times 10^{-6}, \\
&\mathrm{Br}(B \to X_s\ell^+\ell^-)^{\mathrm{SM}}_{q^2\in[14.4,25]\ \mathrm{GeV}^2} \\
&\quad = (2.53 \pm 0.70) \times 10^{-7}, (\ell = e, \mu). \quad (2)
\end{aligned}$$

Moreover, apart from the branching ratio, forward-backward asymmetry (A_{FB}) could also help in the detection of NP scenarios. For this decay process $B \to X_s\ell^+\ell^-(\ell = e, \mu)$ for the two distinct regions of q^2, the experimental values of this observable are given by the Belle Collaboration [16]:

$$\begin{aligned}
&A_{FB}(B \to X_s\ell^+\ell^-)\big|^{\mathrm{exp}}_{q^2\in[1,6]\ \mathrm{GeV}^2} = 0.30 \pm 0.24 \pm 0.04, \\
&A_{FB}(B \to X_s\ell^+\ell^-)\big|^{\mathrm{exp}}_{q^2\in[14.4,25]\ \mathrm{GeV}^2} = 0.28 \pm 0.15 \pm 0.02, \quad (3)
\end{aligned}$$

while the corresponding SM expectations are [16–18]

$$\begin{aligned}
&A_{FB}(B \to X_s\ell^+\ell^-)\big|^{\mathrm{SM}}_{q^2\in[1,6]\ \mathrm{GeV}^2} = -0.07 \pm 0.04, \\
&A_{FB}(B \to X_s\ell^+\ell^-)\big|^{\mathrm{SM}}_{q^2\in[14.4,25]\ \mathrm{GeV}^2} = 0.40 \pm 0.04. \quad (4)
\end{aligned}$$

Therefore, from the above data, it is clearly evident that the SM predictions for the respective observables coincide with the experimental data within a few standard deviations. Hence, by investigating these observables, one can search any favorable NP scenario and also tightly constrain the parameter space of that scenario. With this in mind, in this article we evaluate the decay amplitude for the process $B \to X_s\ell^+\ell^-$ in the nmUED scenario. In literature, one can find several articles, e.g., Refs. [12,19] which have been dedicated to the exploration of the same decay process in the context of several beyond-SM (BSM) scenarios.

In the present article, in order to serve our purposes, we are particularly focused on an extension of SM with one flat spacelike dimension (y) compactified on a circle S^1 of radius R. All the SM fields are allowed to propagate along the extra dimension y. This model is called the five-dimensional (5D) universal extra dimensional (UED) [20] scenario. The fields manifested on this manifold are usually defined in terms of towers of four-dimensional (4D) Kaluza-Klein (KK) states, while the zero mode of the KK towers is designated as the corresponding 4D SM field. A discrete symmetry Z_2 ($y \leftrightarrow -y$) has been needed to generate chiral SM fermions in this scenario. Consequently, the extra dimension is defined as an S^1/Z_2 orbifold, and eventually the physical domain extends from $y = 0$ to $y = \pi R$. As a result, the $y \leftrightarrow -y$ symmetry has been translated as a conserved parity, which is known as KK parity $= (-1)^n$, where n is called the KK number. This KK number (n) is identified as discretized momentum along the y direction. From the conservation of KK parity, the lightest Kaluza-Klein particle (LKP) with KK number one ($n = 1$) cannot decay to a pair of SM particles and becomes absolutely stable. Hence, the LKP has been considered as a potential DM candidate in this scenario [21–28]. Furthermore, a few variants of this model can address some other shortcomings of the SM: for example, gauge coupling unifications [29–31], neutrino mass [32,33], and fermion mass hierarchy [34], etc.

At the nth KK level, all the KK-state particles have the mass $\sqrt{(m^2 + (nR^{-1})^2)}$. Here, m is considered as the zero-mode mass (SM particle mass), which is very small with respect to R^{-1}. Therefore, this UED scenario contains an almost degenerate mass spectrum at each KK level. Consequently, this scenario has lost its phenomenological relevance, specifically, at the colliders. However, this degeneracy in the mass spectrum can be lifted by radiative corrections [35,36]. There are two different types of radiative corrections. The first are considered bulk

[2]The reason for choosing these two regions is given in Sec. III.

[3]These experimental data have also been used in two recent articles [12,13] in the context of the same decay process.

corrections (which are finite and only nonzero for KK excitations of gauge bosons), and the second are regarded as boundary localized corrections that are proportional to logarithmically cutoff-scale-dependent[4] (Λ) terms. The boundary correction terms can be embedded as 4D kinetic, mass, and other possible interaction terms for the KK states at the two fixed boundary points ($y = 0$ and $y = \pi R$) of this orbifold. As a matter of fact, it is very obvious to include such terms in an extra dimensional theory like UED, since these boundary terms have played the role of counterterms for cutoff-dependent loop-induced contributions. In the minimal version of UED (mUED) models, there is an assumption that these boundary terms are tuned in such a way that the 5D radiative corrections exactly vanish at the cutoff scale Λ. However, in general this assumption can be avoided, and without calculating the actual radiative corrections, one might consider the kinetic, mass, and other interaction terms localized at the two fixed boundary points to parametrize these unknown corrections. Therefore, this specific scenario is called nmUED [37–45]. In this scenario, not only the radius of compactification (R), but also the coefficients of different boundary localized terms (BLTs) have been considered as free parameters which can be constrained by various experimental data of different physical observables. In the literature, one can find different such exercises regarding various phenomenological aspects. For example, limits on the values of the strengths of the BLTs have been achieved from the estimation of electroweak observables [43,45]; S, T and U parameters [41,46]; DM relic density [47,48]; production as well as decay of the SM Higgs boson [49]; collider studies of LHC experiments [50–55]; R_b [56]; branching ratios of some rare decay processes, e.g., $B_s \to \mu^+\mu^-$ [7] and $B \to X_s\gamma$ [8]; $\mathcal{R}_{D^{(*)}}$ anomalies [9,57], flavor-changing rare top decay [58,59]; and unitarity of scattering amplitudes involving KK excitations [60].

In this article, we estimate the contributions of KK-excited modes to the decay of $B \to X_s \ell^+ \ell^-$ in a 5D UED model with *nonvanishing* BLT parameters. Our calculation includes next-to-leading-order (NLO) QCD corrections. To the best of our knowledge, this is to be the first article where we will study the decay of $B \to X_s \ell^+ \ell^-$ in the framework of nmUED. Considering the present experimental data of the concerned FCNC process, we will put constraints on the BLT parameters. Furthermore, we would like to investigate how far the lower limit on R^{-1} to higher values can be extended using nonzero BLT parameters. Consequently, it will be an interesting part of this exercise to see whether this lower limit of R^{-1} is comparable with the results obtained from our previous analysis [7,8] or not. Several years ago, the same analysis [61] was performed in the context of a minimal version of the UED model; however, the present experimental data have changed since that time. Therefore, it will be a relevant job to revisit the lower bound on R^{-1} in the UED model by comparing the current experimental result [14,16] with the theoretical estimation using *vanishing* BLT parameters. Furthermore, we estimate the probable bounds on the parameter space of the nmUED scenario by considering the upcoming measurement by the Belle II experiment for the $B \to X_s \ell^+ \ell^-$ decay observables.

In Sec. II, we will give a brief description of the nmUED model. Then in Sec. III, we will show the calculational details of the branching ratio and forward-backward asymmetry for the present process. In Sec. IV, we will present our numerical results. Finally, we conclude the results in Sec. V.

II. KK-PARITY-CONSERVING nmUED SCENARIO: A BRIEF OVERVIEW

Here we present the technicalities of the nmUED scenario required for our analysis. For further discussion regarding this scenario, one can look into Refs. [7–9,37–44,50–56]. In the present scenario, we preserve Z_2 symmetry by considering equal strength of boundary terms at both the boundary points ($y = 0$ and $y = \pi R$). Consequently, KK-parity has been restored in this scenario, which makes the LKP stable. Hence, this present scenario can give a potential DM candidate (such as the first excited KK state of the photon). A comprehensive exercise on DM in nmUED can be found in Ref. [48].

We begin with the action for 5D fermionic fields associated with their boundary localized kinetic term (BLKT) of strength r_f [7–9,42,48]:

$$\begin{aligned} S_{\text{fermion}} = \int d^5x [& \bar{\Psi}_L i\Gamma^M D_M \Psi_L \\ & + r_f\{\delta(y) + \delta(y - \pi R)\}\bar{\Psi}_L i\gamma^\mu D_\mu P_L \Psi_L \\ & + \bar{\Psi}_R i\Gamma^M D_M \Psi_R \\ & + r_f\{\delta(y) + \delta(y - \pi R)\}\bar{\Psi}_R i\gamma^\mu D_\mu P_R \Psi_R], \end{aligned} \tag{5}$$

where $\Psi_L(x, y)$ and $\Psi_R(x, y)$ represent the 5D four component Dirac spinors that can be expressed in terms of two component spinors as [7–9,42,48]

$$\Psi_L(x, y) = \begin{pmatrix} \phi_L(x, y) \\ \chi_L(x, y) \end{pmatrix} = \sum_n \begin{pmatrix} \phi_L^{(n)}(x) f_L^n(y) \\ \chi_L^{(n)}(x) g_L^n(y) \end{pmatrix}, \tag{6}$$

$$\Psi_R(x, y) = \begin{pmatrix} \phi_R(x, y) \\ \chi_R(x, y) \end{pmatrix} = \sum_n \begin{pmatrix} \phi_R^{(n)}(x) f_R^n(y) \\ \chi_R^{(n)}(x) g_R^n(y) \end{pmatrix}. \tag{7}$$

$f_{L(R)}$ and $g_{L(R)}$ are the associated KK wave functions which can be written as the following [7–9,38,43,48]:

[4]UED is considered as an effective theory, and it is characterized by a cutoff scale Λ.

$$f_L^n = g_R^n = N_n^f \begin{cases} \dfrac{\cos\left[m_{f^{(n)}}\left(y-\frac{\pi R}{2}\right)\right]}{\cos\left[\frac{m_{f^{(n)}}\pi R}{2}\right]} & \text{for } n \text{ even}, \\ \dfrac{-\sin\left[m_{f^{(n)}}\left(y-\frac{\pi R}{2}\right)\right]}{\sin\left[\frac{m_{f^{(n)}}\pi R}{2}\right]} & \text{for } n \text{ odd}, \end{cases} \tag{8}$$

and

$$g_L^n = -f_R^n = N_n^f \begin{cases} \dfrac{\sin\left[m_{f^{(n)}}\left(y-\frac{\pi R}{2}\right)\right]}{\cos\left[\frac{m_{f^{(n)}}\pi R}{2}\right]} & \text{for } n \text{ even}, \\ \dfrac{\cos\left[m_{f^{(n)}}\left(y-\frac{\pi R}{2}\right)\right]}{\sin\left[\frac{m_{f^{(n)}}\pi R}{2}\right]} & \text{for } n \text{ odd}. \end{cases} \tag{9}$$

The normalization constant (N_n^f) for the nth KK mode can easily be obtained from the following orthonormality conditions [7–9,48]:

$$\left.\begin{aligned} \int_0^{\pi R} dy[1+r_f\{\delta(y)+\delta(y-\pi R)\}]f_L^m f_L^n \\ \int_0^{\pi R} dy[1+r_f\{\delta(y)+\delta(y-\pi R)\}]g_R^m g_R^n \end{aligned}\right\} = \delta^{nm}, \\ \left.\begin{aligned} \int_0^{\pi R} dy f_R^m f_R^n \\ \int_0^{\pi R} dy g_L^m g_L^n \end{aligned}\right\} = \delta^{nm}, \tag{10}$$

and it takes the form

$$N_n^f = \sqrt{\frac{2}{\pi R}}\left[\frac{1}{\sqrt{1+\frac{r_f^2 m_{f^{(n)}}^2}{4}+\frac{r_f}{\pi R}}}\right]. \tag{11}$$

Here, $m_{f^{(n)}}$ is the KK mass of the nth KK excitation, acquired from the given transcendental equations [7–9,38,48]:

$$\frac{r_f m_{f^{(n)}}}{2} = \begin{cases} -\tan\left(\dfrac{m_{f^{(n)}}\pi R}{2}\right) & \text{for } n \text{ even}, \\ \cot\left(\dfrac{m_{f^{(n)}}\pi R}{2}\right) & \text{for } n \text{ odd}. \end{cases} \tag{12}$$

Let us discuss the Yukawa interactions in this scenario, as the large top quark mass plays a significant role in amplifying the quantum effects in the present study. The action of Yukawa interaction with BLTs of strength r_y is written as [7–9]

$$S_{\text{Yukawa}} = -\int d^5x[\lambda_t^5 \bar{\Psi}_L \tilde{\Phi}\Psi_R + r_y\{\delta(y)+\delta(y-\pi R)\}\lambda_t^5 \bar{\phi}_L \tilde{\Phi}\chi_R + \text{H.c.}]. \tag{13}$$

The 5D coupling strength of Yukawa interaction for the third generation is represented by λ_t^5. Embedding the KK wave functions for fermions [given in Eqs. (6) and (7)] in the actions given in Eqs. (5) and (13), one finds the bilinear terms containing the doublet and singlet states of the quarks. For the nth KK level, the mass matrix can be expressed as the following [7–9]:

$$-\begin{pmatrix} \bar{\phi}_L^{(n)} & \bar{\phi}_R^{(n)} \end{pmatrix}\begin{pmatrix} m_{f^{(n)}}\delta^{nm} & m_t\mathcal{I}_1^{nm} \\ m_t\mathcal{I}_2^{mn} & -m_{f^{(n)}}\delta^{mn} \end{pmatrix}\begin{pmatrix} \chi_L^{(m)} \\ \chi_R^{(m)} \end{pmatrix} + \text{H.c.} \tag{14}$$

Here, m_t is identified as the mass of the SM top quark, while $m_{f^{(n)}}$ is obtained from the solution of the transcendental equations given in Eq. (12). $\mathcal{I}_1^{nm}$ and $\mathcal{I}_2^{nm}$ are the overlap integrals which are given in the following [7–9]:

$$\mathcal{I}_1^{nm} = \left(\frac{1+\frac{r_f}{\pi R}}{1+\frac{r_y}{\pi R}}\right)\int_0^{\pi R} dy[1+r_y\{\delta(y)+\delta(y-\pi R)\}]g_R^m f_L^n,$$

and

$$\mathcal{I}_2^{nm} = \left(\frac{1+\frac{r_f}{\pi R}}{1+\frac{r_y}{\pi R}}\right)\times\int_0^{\pi R} dy g_L^m f_R^n.$$

The integral $\mathcal{I}_1^{nm}$ is nonvanishing for both the conditions of $n=m$ and $n\neq m$. However, for $r_y = r_f$, this integral becomes unity (when $n=m$) or zero ($n\neq m$). On the other hand, the integral $\mathcal{I}_2^{nm}$ is nonvanishing only when $n=m$ and becomes unity in the limit $r_y = r_f$. At this stage, we would like to point out that in our analysis we choose a condition of equality ($r_y = r_f$) to elude the complicacy of mode mixing and develop a simpler form of fermion mixing matrix [7–9,56]. Following this motivation, in the rest of our analysis we will maintain the equality condition[5] $r_y = r_f$.

Implying the alluded equality condition ($r_y = r_f$), the resulting mass matrix [given in Eq. (14)] can readily be diagonalized by following biunitary transformations for the left- and right-handed fields [7–9]:

$$U_L^{(n)} = \begin{pmatrix} \cos\alpha_{tn} & \sin\alpha_{tn} \\ -\sin\alpha_{tn} & \cos\alpha_{tn} \end{pmatrix}, \\ U_R^{(n)} = \begin{pmatrix} \cos\alpha_{tn} & \sin\alpha_{tn} \\ \sin\alpha_{tn} & -\cos\alpha_{tn} \end{pmatrix}, \tag{15}$$

with the mixing angle $\alpha_{tn}\left[=\frac{1}{2}\tan^{-1}\left(\frac{m_t}{m_{f^{(n)}}}\right)\right]$. The gauge eigenstates $\Psi_L(x,y)$ and $\Psi_R(x,y)$ are related with the mass eigenstates T_t^1 and T_t^2 by the given relations [7–9]:

[5]However, in general, one can choose unequal strengths of boundary terms for kinetic and Yukawa interaction for fermions.

$$\phi_L^{(n)} = \cos\alpha_{tn} T_{tL}^{1(n)} - \sin\alpha_{tn} T_{tL}^{2(n)},$$
$$\phi_R^{(n)} = \sin\alpha_{tn} T_{tL}^{1(n)} + \cos\alpha_{tn} T_{tL}^{2(n)},$$
$$\chi_L^{(n)} = \cos\alpha_{tn} T_{tR}^{1(n)} + \sin\alpha_{tn} T_{tR}^{2(n)},$$
$$\chi_R^{(n)} = \sin\alpha_{tn} T_{tR}^{1(n)} - \cos\alpha_{tn} T_{tR}^{2(n)}. \quad (16)$$

Both the physical eigenstates, $T_t^{1(n)}$ and $T_t^{2(n)}$, share the same mass eigenvalue at each KK level. For the nth KK level, it takes the form $M_{t^{(n)}} \equiv \sqrt{m_t^2 + m_{f^{(n)}}^2}$.

In the following, we present the kinetic action [governed by the $SU(2)_L \times U(1)_Y$ gauge group] of 5D gauge and scalar fields with their respective BLKTs [7–9,43,56,58,62]:

$$S_{\text{gauge}} = -\frac{1}{4}\int d^5x [W^a_{MN} W^{aMN} + r_W\{\delta(y)+\delta(y-\pi R)\} W^a_{\mu\nu} W^{a\mu\nu} + B_{MN}B^{MN} + r_B\{\delta(y)+\delta(y-\pi R)\} B_{\mu\nu}B^{\mu\nu}], \quad (17)$$

$$S_{\text{scalar}} = \int d^5x [(D_M\Phi)^\dagger (D^M\Phi) + r_\phi\{\delta(y)+\delta(y-\pi R)\}(D_\mu\Phi)^\dagger (D^\mu\Phi)], \quad (18)$$

where r_W, r_B, and r_ϕ are identified as the strengths of the BLKTs for the respective fields. The 5D field strength tensors are written as

$$W^a_{MN} \equiv (\partial_M W^a_N - \partial_N W^a_M - \tilde{g}_2 \epsilon^{abc} W^b_M W^c_N),$$
$$B_{MN} \equiv (\partial_M B_N - \partial_N B_M). \quad (19)$$

$W^a_M (\equiv W^a_\mu, W^a_4)$ and $B_M (\equiv B_\mu, B_4)$ $(M = 0, 1\ldots 4)$ are represented as the 5D gauge fields corresponding to the gauge groups $SU(2)_L$ and $U(1)_Y$, respectively. The 5D covariant derivative is given as $D_M \equiv \partial_M + i\tilde{g}_2 \frac{\sigma^a}{2} W^a_M + i\tilde{g}_1 \frac{Y}{2} B_M$, where $\tilde{g}_2$ and $\tilde{g}_1$ represent the 5D gauge coupling constants. Here, $\frac{\sigma^a}{2}$ $(a \equiv 1\ldots 3)$ and $\frac{Y}{2}$ are the generators of the $SU(2)_L$ and $U(1)_Y$ gauge groups, respectively. The 5D Higgs doublet is represented by $\Phi = \binom{\phi^+}{\phi^0}$. Each of the gauge and scalar fields which are involved in the above actions [Eqs. (17) and (18)] can be expressed in terms of appropriate KK wave functions as [7–9,56,58,62]

$$V_\mu(x,y) = \sum_n V_\mu^{(n)}(x) a^n(y),$$
$$V_4(x,y) = \sum_n V_4^{(n)}(x) b^n(y), \quad (20)$$

and

$$\Phi(x,y) = \sum_n \Phi^{(n)}(x) h^n(y), \quad (21)$$

where (V_μ, V_4) generically represents both the 5D $SU(2)_L$ and $U(1)_Y$ gauge bosons.

Before proceeding further, we would like to make a few important remarks which could help the reader to understand the following gauge and scalar field structure as well as the corresponding KK wave function. We know that physical neutral gauge bosons generate due to the mixing of B and W^3 fields, and hence the KK decomposition of neutral gauge bosons becomes very intricate in the present extra dimensional scenario because of the existence of two types of mixings both at the bulk as well as on the boundary. Therefore, in this situation without the condition $r_W = r_B$, it would be very difficult to diagonalize the bulk and boundary actions simultaneously by the same 5D field redefinition.[6] Hence, in the following we will sustain the equality condition $r_W = r_B$ [7–9,56,58,62]. Consequently, similar to the mUED scenario, one obtains the same structure of mixing between KK excitations of the neutral component of the gauge fields (i.e., the mixing between $W^{3(n)}$ and $B^{(n)}$) in the nmUED scenario. Therefore, the mixing between $W^{3(1)}$ and $B^{(1)}$ (i.e., the mixing at the first KK level) gives $Z^{(1)}$ and $\gamma^{(1)}$. This $\gamma^{(1)}$ (the first excited KK-state of photon) is absolutely stable by the conservation of KK parity, and it possesses the lowest mass among the first excited KK states in the nmUED particle spectrum. Moreover, it cannot decay to a pair of SM particles. Therefore, this $\gamma^{(1)}$ has played the role of a viable DM candidate in this scenario [48].

In the following, we have given the gauge-fixing action (contains a generic BLKT parameter r_V for gauge bosons) appropriate for the nmUED model [7–9,56,58,62]:

$$S_{\text{gauge fixing}} = -\frac{1}{\xi_y}\int d^5x |\partial_\mu W^{\mu+} + \xi_y(\partial_y W^{4+} + iM_W\phi^+\{1 + r_V(\delta(y)+\delta(y-\pi R))\})|^2 - \frac{1}{2\xi_y}\int d^5x [\partial_\mu Z^\mu + \xi_y(\partial_y Z^4 - M_Z\chi\{1 + r_V(\delta(y)+\delta(y-\pi R))\})]^2 - \frac{1}{2\xi_y}\int d^5x [\partial_\mu A^\mu + \xi_y\partial_y A^4]^2, \quad (22)$$

where $M_W(M_Z)$ is the mass of a SM $W^\pm(Z)$ boson. For a detailed study on the gauge-fixing action/mechanism in nmUED, we refer the reader to Ref. [62]. The above action [given in Eq. (22)] is somewhat intricate and at the same time very crucial for this nmUED scenario, where we will calculate one-loop diagrams (required for the present calculation) in the Feynman gauge. In the presence of

[6]However, in general, one can proceed with $r_W \neq r_B$, but in this situation the mixing between B and W^3 in the bulk and on the boundary points produces off-diagonal terms in the neutral gauge boson mass matrix.

the BLKTs, the Lagrangian leads to a nonhomogeneous weight function for the fields with respect to the extra dimension. This inhomogeneity compels us to define a y-dependent gauge-fixing parameter ξ_y as [7–9,56,58,62]

$$\xi = \xi_y(1 + r_V\{\delta(y) + \delta(y - \pi R)\}), \tag{23}$$

where ξ is not dependent on y. This relation can be treated as *renormalization* of the gauge-fixing parameter, since the BLKTs in some sense play the role of counterterms, taking into account the unknown ultraviolet contribution in loop calculations. In this sense, ξ_y is the bare gauge-fixing parameter, while ξ can be seen as the renormalized gauge-fixing parameter, taking the values 0 (Landau gauge), 1 (Feynman gauge), or ∞ (unitary gauge) [62].

In the present scenario, appropriate gauge-fixing procedure enforces the condition $r_V = r_\phi$ [7–9,56,58,62]. Consequently, KK masses for the gauge and the scalar field are equal [$m_{V^{(n)}} (= m_{\phi^{(n)}})$] and satisfy the same transcendental equation [Eq. (12)]. At the nth KK level, the physical gauge fields ($W^{\mu(n)\pm}$) and charged Higgs ($H^{(n)\pm}$) share the same[7] mass eigenvalue, which is given by [7–9,56,58,62]

$$M_{W^{(n)}} = \sqrt{M_W^2 + m_{V^{(n)}}^2}. \tag{24}$$

Moreover, in the 't Hooft Feynman gauge, the mass of Goldstone bosons ($G^{(n)\pm}$) corresponding to the gauge fields $W^{\mu(n)\pm}$ has the same value $M_{W^{(n)}}$ [7–9,56,58,62].

Additionally, we would like to mention that as in the present article we are dealing with a process that involves off-shell amplitude, we need to use the method of background fields [61,63]. We have already mentioned that the same decay process has already been calculated in Ref. [61] in the context of 5D UED, and further, the authors have also used the same background fields. For this reason, in Appendix A of Ref. [61], the authors have discussed the background field method and also given the corresponding prescription for the 5D UED scenario. We can readily adopt this prescription in the present nmUED scenario because the basic structures of both these models are similar. We hence refrain from providing the details of this method in the present scenario. However, using that prescription (given in Ref. [61]), we can easily evaluate the Feynman rules necessary for our present calculation. In Appendix B of the present article, we give the necessary Feynman rules derived for the 5D background field method in the 5D nmUED scenario in the Feynman gauge.

[7]Similarly, one can find the mass eigenvalues for the KK-excited Z boson and pseudoscalar A. Moreover, their mass eigenvalues are also identical to each other at any KK level. For example, at the nth KK level, they take the form $\sqrt{M_Z^2 + m_{V^{(n)}}^2}$.

We now provide the relevant information of the present scenario up to this point. At this stage, it is important to mention that the interactions for our calculation can be evaluated by integrating out the 5D action over the extra spacelike dimension (y) after plugging in the appropriate y-dependent KK wave function for the respective fields in 5D action. As a consequence, some of the interactions are modified by so-called overlap integrals with respect to their mUED counterparts. The expressions of the overlap integrals have been given in Appendix B. For further information on these overlap integrals we refer the reader to Ref. [7].

III. $B \to X_s\ell^+\ell^-$ IN nmUED

The semileptonic inclusive decay $B \to X_s\ell^+\ell^-$ is quite suppressed in the SM; however, it is very compelling for finding a NP signature. Therefore, several B physics experimental collaborations (Belle, *BABAR*) have been involved to measure several observables (mainly decay branching ratio and forward-backward asymmetry) associated with this decay process. In the context of SM, the dominant perturbative contribution has been evaluated in Ref. [64], and later two-loop QCD corrections[8] have been described in Refs. [68,69]. Since in this particular decay mode, a lepton-antilepton pair is present, more structures contribute to the decay rate and some subtleties arise in the theoretical description for this process. For the decay to be dominated by perturbative contributions, one has to eliminate $c\bar{c}$ resonances that show up as large peaks in the dilepton invariant mass spectrum by the judicious choice of kinematic cuts. Consequently, this leads to "perturbative dilepton invariant mass windows," namely, the low dilepton mass region $1\ \text{GeV}^2 < q^2 < 6\ \text{GeV}^2$, and also the high dilepton mass region with $q^2 > 14.4\ \text{GeV}^2$.

In this section, we will describe the details of the calculation of the branching ratio and the forward-backward asymmetry of $B \to X_s\ell^+\ell^-$ in the nmUED model. Since the basic gauge structure of the present nmUED model is similar to that of the SM, leading-order (LO) contributions to electroweak dipole operators are one-loop suppressed as in the SM. However, in the present model, due to the presence of a large number of KK particles, we encounter more one-loop diagrams in comparison to the SM. Hence, we will evaluate the total contributions of these KK particles to the electroweak dipole operators

[8]Research regarding higher-order perturbative contributions has been studied extensively and has already reached a high level of accuracy. For example, one can find NNLO QCD corrections in Ref. [65], and Refs. [66,67] include QED corrections. Moreover, updated analysis of all angular observables in the $B \to X_s\ell^+\ell^-$ decay has been given in Ref. [15]. It also contains all available perturbative NNLO QCD and NLO QED corrections and includes subleading power corrections.

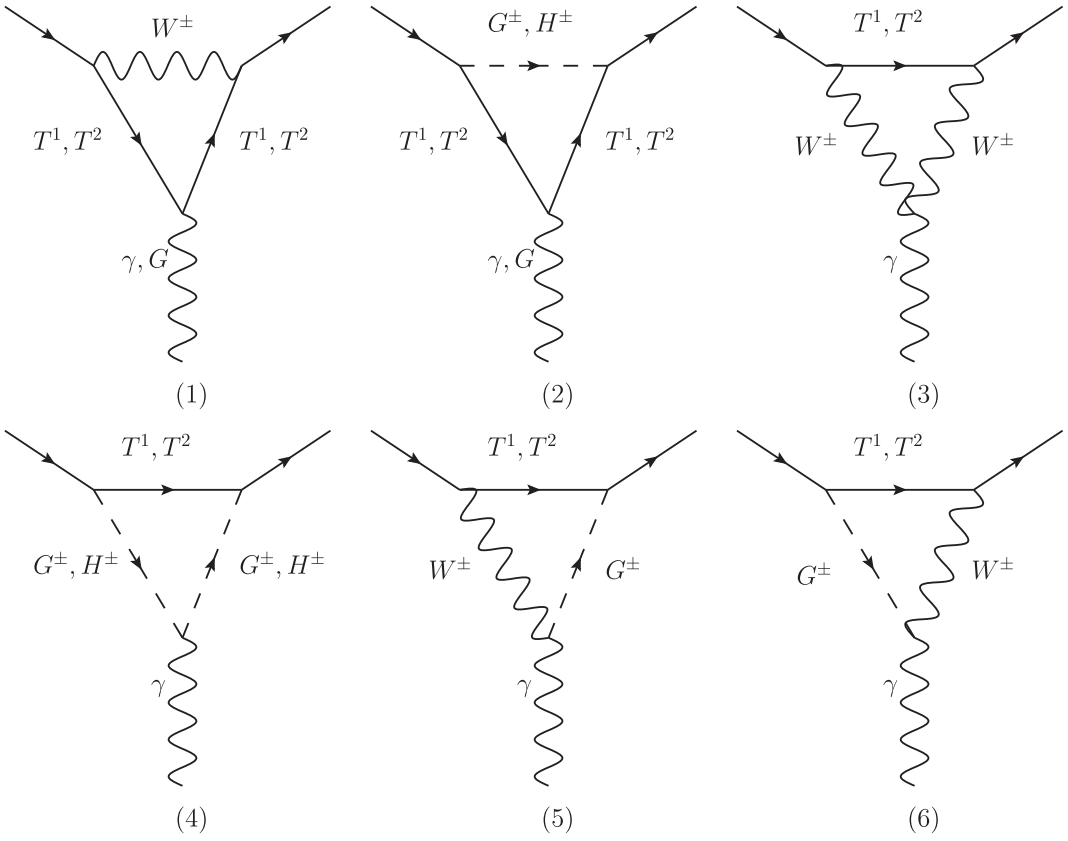

FIG. 1. Relevant electroweak penguin diagrams contributing to the decay of $B \to X_s \ell^+ \ell^-$.

and simply add them to the SM contribution. With this spirit, following the same technique as in Ref. [61], we will evaluate the relevant WCs of the electroweak dipole operators at the LO level. Then, following the prescription given in Refs. [68,69], we will include the NLO QCD correction in the concerned decay process.

A. Effective Hamiltonian for $B \to X_s \ell^+ \ell^-$

The effective Hamiltonian for the decay $B \to X_s \ell^+ \ell^-$ at hadronic scales $\mu = \mathcal{O}(m_b)$ can be written as [61]

$$\mathcal{H}_{\rm eff}(b \to s\ell^+\ell^-) = \mathcal{H}_{\rm eff}(b \to s\gamma) - \frac{G_{\rm F}}{\sqrt{2}} V_{ts}^* V_{tb} \times [C_{9V}(\mu) Q_{9V} + C_{10A}(M_W) Q_{10A}], \tag{25}$$

where G_F represents the Fermi constant and V_{ij} are the elements of the Cabibbo-Kobayashi-Maskawa (CKM) matrix. In the above expression [Eq. (25)], apart from the relevant operators[9] for $B \to X_s\gamma$, there are two new operators [61]:

$$Q_{9V} = (\bar{s}b)_{V-A}(\bar{\ell}\ell)_V, \qquad Q_{10A} = (\bar{s}b)_{V-A}(\bar{\ell}\ell)_A, \tag{26}$$

where V and A refer to the vector and axial-vector current, respectively. They are produced via the electroweak penguin diagrams shown in Fig. 1, and the other relevant Feynman diagrams needed to maintain gauge invariance (for the nmUED scenario) have been given in Ref. [7].

For the purpose of convenience, the above WCs [given in Eq. (25)] can be defined in terms of two new coefficients, $\tilde{C}_9$ and $\tilde{C}_{10}$, as [61,69]

$$C_{9V}(\mu) = \frac{\alpha}{2\pi} \tilde{C}_9(\mu), \tag{27}$$

$$C_{10A}(\mu) = \frac{\alpha}{2\pi} \tilde{C}_{10}(\mu), \tag{28}$$

where

$$\tilde{C}_{10}(\mu) = -\frac{Y(x_t, r_f, r_V, R^{-1})}{\sin^2\theta_w}. \tag{29}$$

The function $Y(x_t, r_f, r_V, R^{-1})$ in the context of the nmUED scenario has been calculated in Ref. [7]. θ_w is the Weinberg angle, and α represents the fine structure constant. The operator Q_{10A} does not evolve under QCD renormalization, and its coefficient is independent of μ.

[9]The explicit form of the effective Hamiltonian for $b \to s\gamma$ is given in Refs. [8,61].

On the other hand, using the results of NLO QCD corrections to $\tilde{C}_9(\mu)$ in the SM given in Refs. [68,69], we can readily obtain this coefficient in the present nmUED model under the naive dimensional regularization (NDR) renormalization scheme as

$$\begin{aligned}\tilde{C}_9^{\rm eff}(q^2) &= \tilde{C}_9^{\rm NDR}\tilde{\eta}\left(\frac{q^2}{m_b^2}\right) + h\left(z,\frac{q^2}{m_b^2}\right)(3C_1^{(0)} + C_2^{(0)} \\ &\quad + 3C_3^{(0)} + C_4^{(0)} + 3C_5^{(0)} + C_6^{(0)}) \\ &\quad - \frac{1}{2}h\left(1,\frac{q^2}{m_b^2}\right)(4C_3^{(0)} + 4C_4^{(0)} + 3C_5^{(0)} + C_6^{(0)}) \\ &\quad - \frac{1}{2}h\left(0,\frac{q^2}{m_b^2}\right)(C_3^{(0)} + 4C_4^{(0)}) \\ &\quad + \frac{2}{9}(3C_3^{(0)} + C_4^{(0)} + 3C_5^{(0)} + C_6^{(0)}),\end{aligned} \tag{30}$$

where

$$\begin{aligned}\tilde{C}_9^{\rm NDR}(\mu) &= P_0^{\rm NDR} + \frac{Y(x_t, r_f, r_V, R^{-1})}{\sin^2\theta_w} \\ &\quad - 4Z(x_t, r_f, r_V, R^{-1}) + P_E E(x_t, r_f, r_V, R^{-1}).\end{aligned} \tag{31}$$

The value[10] of $P_0^{\rm NDR}$ is 2.60 ± 0.25 [61], and P_E is $\mathcal{O}(10^{-2})$ [69]. Using the relation given in Refs. [61,69], we can express the function Z in the nmUED scenario as

$$\begin{aligned}&Z(x_t, r_f, r_V, R^{-1}) \\ &\quad = C(x_t, r_f, r_V, R^{-1}) + \frac{1}{4}D(x_t, r_f, r_V, R^{-1}),\end{aligned} \tag{32}$$

while the function $C(x_t, r_f, r_V, R^{-1})$ for the nmUED scenario has been calculated in Ref. [7]. The function $\tilde{\eta}$ given in Eq. (30) represents single-gluon corrections to the matrix element Q_9, and it takes the form [69]

$$\tilde{\eta}\left(\frac{q^2}{m_b^2}\right) = 1 + \frac{\alpha_s}{\pi}\omega\left(\frac{q^2}{m_b^2}\right), \tag{33}$$

where α_s is the QCD fine structure constant. The explicit forms of the functions ω, h, and other WCs [e.g., as given in Eq. (30)] required for the present decay process have been given in Appendix A. The functions $D(x_t, r_f, r_V, R^{-1})$ and $E(x_t, r_f, r_V, R^{-1})$, which we evaluate in this article, are given in the following form:

$$D(x_t, r_f, r_V, R^{-1}) = D_0(x_t) + \sum_{n=1}^{\infty} D_n(x_t, x_{f^{(n)}}, x_{V^{(n)}}) \tag{34}$$

and

$$E(x_t, r_f, r_V, R^{-1}) = E_0(x_t) + \sum_{n=1}^{\infty} E_n(x_t, x_{f^{(n)}}, x_{V^{(n)}}), \tag{35}$$

with $x_t = \frac{m_t^2}{M_W^2}$, $x_{V^{(n)}} = \frac{m_{V^{(n)}}^2}{M_W^2}$, and $x_{f^{(n)}} = \frac{m_{f^{(n)}}^2}{M_W^2}$. $m_{V^{(n)}}$ and $m_{f^{(n)}}$ can be obtained from the transcendental equation given in Eq. (12). The functions $D_0(x_t)$ and $E_0(x_t)$ are the corresponding SM contributions at the electroweak scale [61,68–71]:

$$D_0(x_t) = -\frac{4}{9}\ln x_t + \frac{-19x_t^3 + 25x_t^2}{36(x_t-1)^3} + \frac{x_t^2(5x_t^2 - 2x_t - 6)}{18(x_t-1)^4}\ln x_t, \tag{36}$$

$$\begin{aligned}E_0(x_t) &= -\frac{2}{3}\ln x_t + \frac{x_t^2(15 - 16x_t + 4x_t^2)}{6(1-x_t)^4}\ln x_t \\ &\quad + \frac{x_t(18 - 11x_t - x_t^2)}{12(1-x_t)^3}.\end{aligned} \tag{37}$$

Now, we will depict the nmUED contribution to the electroweak penguin diagrams. We have already mentioned that the KK masses and couplings involving KK excitations are nontrivially modified with respect to their UED counterparts due to the presence of different BLTs in the nmUED action. Therefore, it would not be possible to obtain the expressions of the D and E functions in nmUED simply by rescaling the results of the UED model [61]. Consequently, we have evaluated the functions $D_n(x_t, x_{f^{(n)}}, x_{V^{(n)}})$ and $E_n(x_t, x_{f^{(n)}}, x_{V^{(n)}})$ *independently* for the nmUED scenario. These functions (D_n and E_n) represent the KK contributions for the nth KK mode which are computed from the electroweak penguin diagrams (given in Fig. 1) in the nmUED model for photons and gluons, respectively. Furthermore, it is quite evident from Eqs. (38) and (39) that they are remarkably different from those of the UED expression [given in Eqs. (3.31) and (3.32) of Ref. [61]]. However, from our expressions [given in Eqs. (38) and (39)], we can reconstruct the results of the UED version [given in Eqs. (3.31) and (3.32) of the Ref. [61]] if we set the boundary terms to zero; i.e., r_f, $r_V = 0$.

To this end, we would like to mention that in our calculation of one-loop penguin diagrams (in order to measure the contributions of KK excitation to the decay of $B \to X_s\ell^+\ell^-$), we consider only those interactions which couple a zero-mode field to a pair of KK excitations carrying equal KK number. Even so, in the nmUED scenario due to KK-parity conservation, one can also have nonzero interactions involving KK excitations with KK numbers n, m and p, where $n + m + p$ is an even integer. However, we have explicitly checked that the final results would not change remarkably even if one considers the contributions of all the possible off-diagonal interactions [7,8,56].

[10]The analytic formula for $P_0^{\rm NDR}$ has been given in Ref. [69].

For the nth KK level, the electroweak *photon* penguin function (which is obtained from penguin diagrams given in Fig. 1) takes the form

$$\begin{aligned}
D_n(x_t, x_{f^{(n)}}, x_{V^{(n)}}) = &\frac{2}{3}E_n(x_t, x_{f^{(n)}}, x_{V^{(n)}}) - \frac{1}{36(-1+x_{f^{(n)}}-x_{V^{(n)}})^4}\Big[(-1+x_{f^{(n)}}-x_{V^{(n)}})\{-2(I_1^n)^2(43x_{f^{(n)}}^2 - 65x_{f^{(n)}}(1+x_{V^{(n)}}) \\
&+16(1+x_{V^{(n)}})^2) + (I_2^n)^2(11x_{f^{(n)}}^2 - 7x_{f^{(n)}}(1+x_{V^{(n)}}) + 2(1+x_{V^{(n)}})^2)\} \\
&-6x_{f^{(n)}}^2\{(I_2^n)^2 x_{f^{(n)}} + 2(I_1^n)^2(6-5x_{f^{(n)}}+6x_{V^{(n)}})\}\ln\left(\frac{x_{f^{(n)}}}{1+x_{V^{(n)}}}\right)\Big] \\
&+\frac{1}{36(-1+x_t+x_{f^{(n)}}-x_{V^{(n)}})^4}\Big[(-1+x_t+x_{f^{(n)}}-x_{V^{(n)}})\{(I_1^n)^2(11x_t^3 + x_{f^{(n)}}^2(-86+11x_t) - x_t^2(93+7x_{V^{(n)}}) \\
&+32(1+x_{V^{(n)}})^2 + 2x_t(1+x_{V^{(n)}})(66+x_{V^{(n)}}) + x_{f^{(n)}}(x_t(-179+22x_t-7x_{V^{(n)}})130(1+x_{V^{(n)}}))) \\
&+(I_2^n)^2(11x_{f^{(n)}}^2 + 11x_t^2 - 7x_t(1+x_{V^{(n)}}) + 2(1+x_{V^{(n)}})^2 + x_{f^{(n)}}(22x_t - 7(1+x_{V^{(n)}})))\} \\
&-6(x_t+x_{f^{(n)}})^2\{(I_2^n)^2(x_t+x_{f^{(n)}}) + (I_1^n)^2((x_t+x_{f^{(n)}})(-10+x_t) + 12(1+x_{V^{(n)}}))\}\ln\left(\frac{x_t+x_{f^{(n)}}}{1+x_{V^{(n)}}}\right)\Big], \qquad (38)
\end{aligned}$$

while the function $E_n(x_t, x_{f^{(n)}}, x_{V^{(n)}})$ is regarded as the corresponding contribution for *gluon* penguins given by the first two diagrams of Fig. 1. The expression of the function $E_n(x_t, x_{f^{(n)}}, x_{V^{(n)}})$ in nmUED is given as the following:

$$\begin{aligned}
E_n(x_t, x_{f^{(n)}}, x_{V^{(n)}}) = &-\frac{1}{36(-1+x_{f^{(n)}}-x_{V^{(n)}})^4}\Big[(-1+x_{f^{(n)}}-x_{V^{(n)}})\{(I_1^n)^2(50x_{f^{(n)}}^2 - 58x_{f^{(n)}}(1+x_{V^{(n)}}) - 4(1+x_{V^{(n)}})^2) \\
&+(I_2^n)^2(7x_{f^{(n)}}^2 - 29x_{f^{(n)}}(1+x_{V^{(n)}}) + 16(1+x_{V^{(n)}})^2)\} - 6(1+x_{V^{(n)}})\{(I_2^n)^2(1+x_{V^{(n)}})(2-3x_{f^{(n)}}+2x_{V^{(n)}}) \\
&+2(I_1^n)^2(6x_{f^{(n)}}^2 - 9x_{f^{(n)}}(1+x_{V^{(n)}}) + 2(1+x_{V^{(n)}})^2)\}\ln\left(\frac{x_{f^{(n)}}}{1+x_{V^{(n)}}}\right)\Big] \\
&+\frac{1}{36(-1+x_t+x_{f^{(n)}}-x_{V^{(n)}})^4}\Big[(-1+x_t+x_{f^{(n)}}-x_{V^{(n)}})\{(I_1^n)^2(7x_t^3 + x_{f^{(n)}}^2(50+7x_t) + x_t^2(21-29x_{V^{(n)}}) \\
&-4(1+x_{V^{(n)}})^2 + 2x_t(1+x_{V^{(n)}})(-21+8x_{V^{(n)}}) + x_{f^{(n)}}(-58+71x_t+14x_t^2 - 29(2+x_t)x_{V^{(n)}})) \\
&+(I_2^n)^2(7x_{f^{(n)}}^2 + 7x_t^2 - 29x_t(1+x_{V^{(n)}}) + 16(1+x_{V^{(n)}})^2 + x_{f^{(n)}}(14x_t - 29(1+x_{V^{(n)}})))\} \\
&-6(1+x_{V^{(n)}})\{(I_2^n)^2(1+x_{V^{(n)}})(2-3x_{f^{(n)}}-3x_t+2x_{V^{(n)}}) + (I_1^n)^2(12x_{f^{(n)}}^2 - 3x_t^2(-3+x_{V^{(n)}}) \\
&+2x_t(-8+x_{V^{(n)}})(1+x_{V^{(n)}}) + 4(1+x_{V^{(n)}})^2 - 3x_{f^{(n)}}(6-7x_t+(6+x_t)x_{V^{(n)}}))\}\ln\left(\frac{x_t+x_{f^{(n)}}}{1+x_{V^{(n)}}}\right)\Big]. \qquad (39)
\end{aligned}$$

In the above expressions, I_1^n and I_2^n represent overlap integrals whose analytic forms have been given in Appendix B [see Eqs. (B10) and (B11)].

B. The differential decay rate

We are now in a stage where, on the basis of the effective Hamiltonian given in Eq. (25), we can readily define the differential decay rate in the NDR scheme [68,69]:

$$\begin{aligned}
R(q^2) &\equiv \frac{1}{\Gamma(b\to ce\bar{\nu})}\frac{d\Gamma(b\to s\ell^+\ell^-)}{dq^2} \\
&= \frac{\alpha^2}{4\pi^2}\left|\frac{V_{ts}^* V_{tb}}{V_{cb}}\right|^2 \frac{(1-\frac{q^2}{m_b^2})^2}{f(z)\kappa(z)}U(q^2). \qquad (40)
\end{aligned}$$

Here,

$$f(z) = 1 - 8z^2 + 8z^6 - z^8 - 24z^4\ln(z) \qquad (41)$$

is the phase-space factor, and

$$\kappa(z) \simeq 1 - \frac{2\alpha_s(\mu)}{3\pi}\left[\left(\pi^2 - \frac{31}{4}\right)(1-z)^2 + \frac{3}{2}\right] \qquad (42)$$

represents the single-gluon QCD correction to $b \to ce\bar{\nu}$ decay [72,73], with $z = \frac{m_c}{m_b}$. The function $U(q^2)$ is expressed as

$$U(q^2) = \left(1+\frac{2q^2}{m_b^2}\right)(|\tilde{C}_9^{\rm eff}(q^2)|^2 + |\tilde{C}_{10}|^2) + 4\left(1+\frac{2m_b^2}{q^2}\right)|C_{7\gamma}^{(0)\rm eff}|^2 + 12 C_{7\gamma}^{(0)\rm eff}{\rm Re}\tilde{C}_9^{\rm eff}(q^2), \tag{43}$$

where $\tilde{C}_9^{\rm eff}(q^2)$ is given in Eq. (30). The explicit formula for $C_{7\gamma}^{(0)\rm eff}$ is shown in Appendix A. Among the several terms given in Eq. (43), $|\tilde{C}_9^{\rm eff}(q^2)|^2$ is almost similar to that of the SM, and $|\tilde{C}_{10}|^2$ is appreciably enhanced; however, the last two terms are suppressed. Furthermore, the last term in Eq. (43) is negative, and hence its suppression results are responsible for an enhancement of $U(q^2)$ in addition to the one due to $\tilde{C}_{10}$. Using Eq. (40), one can easily evaluate the branching ratio for the present decay process for a given range of q^2. In the numerical calculations, we will use the value 0.104 for ${\rm Br}(B \to X_c e\bar{\nu})_{\rm exp}$.

C. Forward-backward asymmetry

For the present decay process $B \to X_s \ell^+\ell^-$, another observable, called forward-backward asymmetry, could be instrumental for the detection of NP scenarios. It is nonzero only at the NLO level. The un-normalized expression is given as [74]

$$\bar{A}_{FB}(q^2) \equiv \frac{1}{\Gamma(b\to ce\bar{\nu})}\int_{-1}^{1} d\cos\theta_\ell \frac{d^2\Gamma(b\to s\ell^+\ell^-)}{dq^2 d\cos\theta_\ell} \times {\rm sgn}(\cos\theta_l), \tag{44}$$

$$= -3\frac{\alpha^2}{4\pi^2}\left|\frac{V_{ts}^* V_{tb}}{V_{cb}}\right|^2 \frac{(1-\frac{q^2}{m_b^2})^2}{f(z)\kappa(z)}\tilde{C}_{10}\left[\frac{q^2}{m_b^2}{\rm Re}\tilde{C}_9^{\rm eff}(q^2) + 2C_{7\gamma}^{(0)\rm eff}\right]. \tag{45}$$

Here, θ_ℓ represents the angle of the ℓ^+ with respect to b quark direction in the center-of-mass system of the dilepton pair. The normalized form can be expressed as

$$A_{FB} = \frac{\bar{A}_{FB}(q^2)}{R(q^2)}, \tag{46}$$

while the global forward-backward asymmetry in a region $q^2 \in [a,b]$ GeV^2 can be defined as [12,19]

$$A_{FB}|_{q^2\in[a,b]\ {\rm GeV}^2} = \frac{\int_a^b dq^2 \bar{A}_{FB}(q^2)}{\int_a^b dq^2 R(q^2)}. \tag{47}$$

In the following section, we will present the numerical estimation of these observables for the allowed parameter space in the nmUED scenario.

IV. ANALYSIS AND RESULTS

The effective Hamiltonian [given in Eq. (25)] required for the decay $B \to X_s\ell^+\ell^-$ contains different WCs, and in our analysis we evaluate KK contributions to each of these coefficients at each KK level. In this article, for the first time we have calculated the KK contributions to the coefficients of electroweak dipole operators in the nmUED scenario. The functions $D_n(x_t, x_{f^{(n)}}, x_{V^{(n)}})$ [given in Eq. (38)] and $E_n(x_t, x_{f^{(n)}}, x_{V^{(n)}})$ [given in Eq. (39)] represent the nth-level KK contributions to the coefficients for the dipole operators for photons and gluons, respectively. These functions (D_n and E_n) depend on gauge bosons as well as fermion KK masses[11] in the nmUED scenario. Furthermore, other coefficients needed for the concerned decay process in the nmUED scenario have been given in our previous articles [7,8]. At this point, we would like to mention that, considering the analysis of the effect of SM Higgs mass on vacuum stability in the UED model [76], we sum the KK contributions up to 5 KK levels,[12] and finally we add up the total KK contributions with the SM counterpart. In fact, we have explicitly checked that the numerical values would not differ remarkably, as the sum over the KK modes, in this case, is converging[13] in nature. More specifically, during the calculation of loop diagrams, the summation of KK levels becomes saturated after the consideration of a certain number of KK levels. Consequently, the final results would not change significantly whether we consider 5 KK levels or 20 KK levels during the evaluation of KK contributions for the loop diagrams. In support of our assumption, at the end of the following subsection, we will present two tables (Tables II and III) which will ensure the insensitivity on the number of KK levels in summation.

TABLE I. Experimental values for branching ratios of $B_s \to \mu^+\mu^-$ and $B \to X_s\gamma$.

Process	Experimental value of branching ratio
$B_s \to \mu^+\mu^-$	$(2.8^{+0.8}_{-0.7}) \times 10^{-9}$ [78]
$B \to X_s\gamma$	$(3.32 \pm 0.16) \times 10^{-4}$ [79]

A. Constraints and choice of range of BLT parameters

Here we briefly discuss the following constraints that have been imposed in our analysis:

(1) Several rare decay processes, for example $B_s \to \mu^+\mu^-$ and $B \to X_s\gamma$, have always been very crucial for searching any favorable kind of NP scenario. The latest experimental values for branching ratios of these processes are given in Table I. In the context of the nmUED scenario, thorough analyses on the

[11] We use $M_W = 80.38$ GeV for the SM $W^\pm$ gauge boson mass and $m_t = 173.1$ GeV for the SM top quark mass as given in Ref. [75].

[12] Analysis in earlier articles used 20–30 KK levels while adding up the contributions from KK modes.

[13] The summation of the KK contribution is convergent in UED-type models with one extra spacelike dimension, as far as one-loop calculation is concerned [77].

two rare decay processes mentioned in Table I have been performed in Refs. [7] and [8], respectively. Using the expressions of $\mathrm{Br}(B_s \to \mu^+\mu^-)$ and $\mathrm{Br}(B \to X_s\gamma)$ given in Refs. [7] and [8], we have treated the branching ratios of these rare decay processes as constraints in our present analysis.

(2) The electroweak precision test (EWPT) is an essential and important tool for constraining any form of BSM physics. In the nmUED model, corrections to the Peskin-Takeuchi parameters S, T, and U appear via the correction to the Fermi constant G_F at tree level. This is a remarkable contrast with respect to the minimal version of the UED model, where these corrections appear via one-loop processes. Detailed study on EWPT for the present version of the nmUED model has been provided in Refs. [7,9]. Following the same approach given in Refs. [7,9], we have applied EWPT as one of the constraints in our analysis.

To this end, we would like to mention the range of values of BLT parameters used in our analysis. In general, BLT parameters may be positive or negative. However, it is readily evident from Eq. (11) that for $r_f/R = -\pi$ the

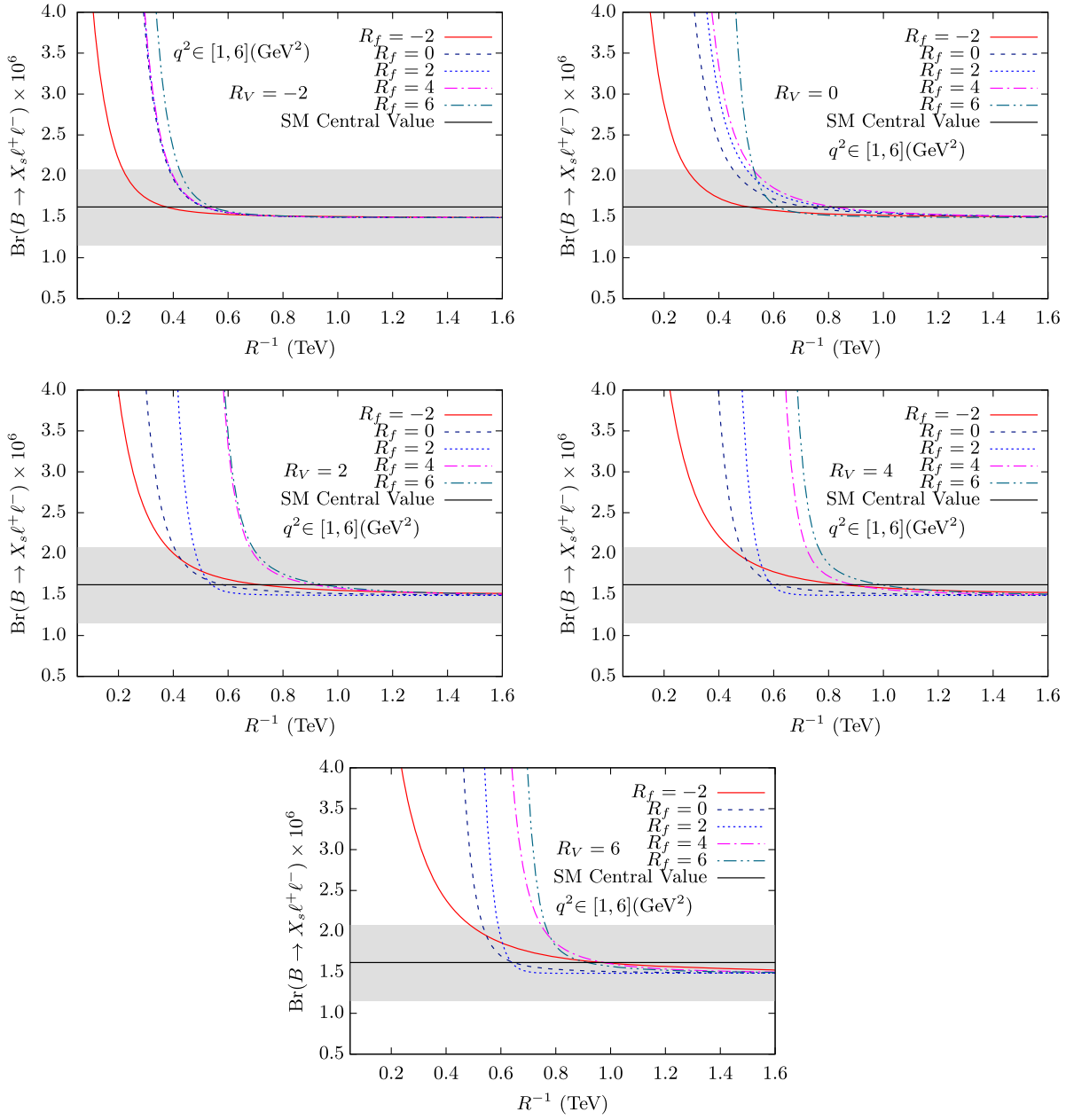

FIG. 2. Variation of the branching ratio of $B \to X_s\ell^+\ell^-$ with R^{-1} (TeV) for various values of $R_f(= r_f/R)$. The five panels represent different values of $R_V(= r_V/R)$. We sum the contributions up to five KK levels in different loop functions while calculating WCs. The horizontal gray band depicts the 1σ allowed range of the experimental value of the branching ratio for $q^2 \in [1,6]$ GeV^2.

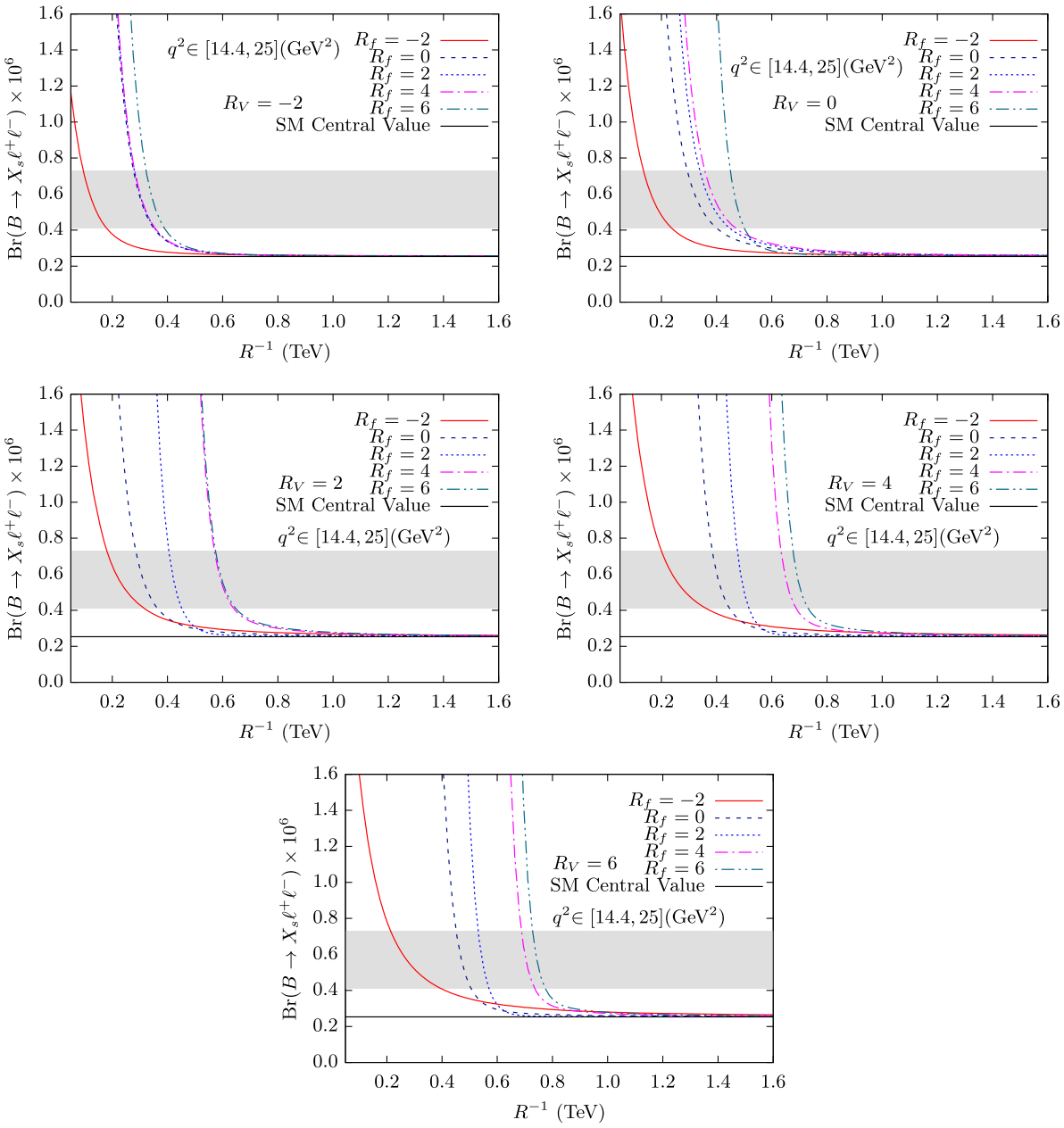

FIG. 3. Variation of the branching ratio of $B \to X_s \ell^+ \ell^-$ with R^{-1} (TeV) for various values of $R_f (= r_f/R)$. The five panels represent different values of $R_V (= r_V/R)$. We sum the contributions up to five KK levels in different loop functions while calculating WCs. The horizontal gray band depicts the 1σ allowed range of experimental value of the branching ratio for $q^2 \in [14.4, 25]$ GeV^2.

zero-mode solution becomes divergent, and beyond $r_f/R = -\pi$ the zero-mode fields become ghostlike. Hence, any values of BLT parameters less than $-\pi R$ should be discarded, although for the sake of completeness we have shown numerical results for some negative BLT parameters. However, analysis of electroweak precision data [7,9] disfavors a large portion of negative BLT parameters.

B. Numerical results

We are in a position where we would like to present the primary results of our analysis.

1. Branching ratio

In Figs. 2 and 3, we have depicted the variation of the branching ratio of $B \to X_s \ell^+ \ell^-$ as a function of scaled BLT parameters ($R_V \equiv r_V/R$ and $R_f \equiv r_f/R$) and the inverse of the radius of compactification (R^{-1}) for two different dilepton mass-squared regions $q^2 \in [1, 6]$ GeV^2 and $q^2 \in [14.4, 25]$ GeV^2, respectively. We have mentioned earlier that nonvanishing BLT parameters nontrivially modify the KK masses and various couplings among the KK excitations in the nmUED scenario. Therefore, in the following we will discuss how these BLT parameters affect

TABLE II. Lower limits on R^{-1} (in GeV) evaluated from the branching ratio of $B \to X_s \ell^+ \ell^-$ for several values of BLT parameters for $q^2 \in [1, 6]$ GeV^2, showing the insensitivity on the number of KK modes in summation.

	$R_V = -2$		$R_V = 0$		$R_V = 2$		$R_V = 4$		$R_V = 6$	
R_f	5 KK level	20 KK level	5 KK level	20 KK level	5 KK level	20 KK level	5 KK level	20 KK level	5 KK level	20 KK level
−2	215.73	224.19	283.62	289.23	377.06	381.14	437.53	443.33	487.00	489.26
0	382.15	388.95	451.27	464.93	472.55	482.32	478.76	485.35	530.98	549.54
2	385.45	392.72	498.00	508.18	510.01	518.05	536.48	548.76	588.70	598.28
4	390.26	394.83	525.48	529.81	676.65	688.72	717.88	726.93	745.36	750.21
6	421.04	430.52	528.23	533.45	684.89	694.54	761.85	768.14	764.60	770.42

the concerned decay process. For each of the q^2 regions we present five panels, corresponding to five different values of the scaled gauge BLT parameter R_V. In each panel, we show the dependence of the branching ratio with R^{-1} for five different values of the scaled fermion BLT parameter R_f.

If we focus on a particular curve specified by R_V and R_f, then we observe that the branching ratio monotonically decreases with respect to increasing values of R^{-1}. It is quite expected in a scenario like nmUED, where the masses of KK-excited states are basically characterized by R^{-1}; i.e., with increasing values of R^{-1}, the masses of KK-excited states are increased. Therefore, with increasing values of KK masses, the one-loop functions involved in this decay process are suppressed, which in turn decreases the decay width (and branching ratio). Further, depending on the BLT parameters, after a certain value of R^{-1}, the branching ratio asymptotically converges to its SM value as $R^{-1} \to \infty$. This behavior clearly indicates the decoupling behavior of the KK-mode contribution.

Moreover, it is clearly evident from Figs. 2 and 3 that branching ratio of $B \to X_s \ell^+ \ell^-$ increases with the increment of both of the BLT parameters. For example, if we concentrate on a particular panel specified by a fixed value of R_V, then one can see that with increasing values of R_f, the branching ratio is enhanced. The reason is that, with increasing values of R_f, KK-fermion masses decrease, and consequently the loop functions are enhanced. Therefore, the branching ratio increases with higher values of R_f. At the same time, if we look at all the panels of any particular figure (either Fig. 2 or Fig. 3), then we will readily conclude that the other BLT parameter R_V affects the branching ratio in a similar manner to R_f. However, the branching ratio is a bit extra sensitive to the variation of R_f rather than R_V. This can be explained by observing the interactions which are involved in this calculation listed in Appendix B. As per earlier discussion (see the paragraph before the beginning of Sec. III), the interactions are modified by the overlap integrals I_1^n and I_2^n. I_1^n modify the interactions of third generations of quarks with charged Higgs scalar ($H^{(n)\pm}$) and gauge bosons ($W^{(n)\pm}$), while the interactions between the fifth component of W bosons and third generations of quarks are modified by I_2^n. Therefore, due to the combined effects of the top-Yukawa coupling and $SU(2)$ gauge interaction, I_1^n dominates over I_2^n, which is controlled by $SU(2)$ gauge interaction only. Hence, R_f has a better control on the $B \to X_s \ell^+ \ell^-$ amplitude (via I_1^n) than R_V.

At this point, we would like to comment on the values of BLT parameters. It is clearly evident from Figs. 2 and 3 that negative values of BLT parameters are not very encouraging for the present purpose, because we cannot get any strong lower limit on R^{-1}. For negative BLT parameters, the KK masses are larger with respect to positive BLT parameters. Therefore, enhanced KK mass suppresses the loop functions, and consequently decay amplitude decreases. Apart from this, the constraint of EWPT would prefer larger values of R^{-1} for negative BLT parameters [7,9]. Hence, in the case of our present purpose, the positive values of BLT parameters are more preferable. For example, for $q^2 \in [1, 6]$ GeV^2, if we choose $R_V = 2$, $R_f = 6$, $R^{-1} > 680$ (690) GeV (see Table II) when we consider the sum up to 5 (20) KK levels. On the other hand, the lower limit on R^{-1} changes to > 760 (770) GeV for $R_f = R_V = 6$ (see Table II). In the case of the other region of $q^2 (\in [14.4, 25]$ GeV$^2)$, the lower limits on R^{-1} for the above mentioned BLT parameters change to > 570 (580) GeV (see Table III) and > 720 (730) GeV (see Table III), respectively, for the KK sum up to 5 (20) levels. We have obtained these limits on R^{-1} by comparing the branching ratio evaluated from the present calculation to the experimental data [given in Eq. (1)] with a 1σ upward error bar. From these numbers, we find that the limits are slightly better than that of the results obtained from the analysis $B \to X_s \gamma$ [8]; however, they are in the same ballpark as those obtained from the analysis of $B_s \to \mu^+ \mu^-$ [7]. Furthermore, if we look at Figs. 2 and 3 (or Tables II and III), then we find that the lower limits on R^{-1} would not drastically change after certain positive values of BLT parameters. For example, in the present analysis we have restricted ourselves for the choice of BLT parameters (both R_V and R_f) to values up to 6. The reason is that beyond this choice, we expect that the lower limit on R^{-1} would not change significantly for larger values of BLT parameters.

In Tables II and III (for two different regions of q^2), we have enlisted specific values of lower limits on R^{-1}

TABLE III. Lower limits on R^{-1} (in GeV) evaluated from the branching ratio of $B \to X_s \ell^+ \ell^-$ for several values of BLT parameters for $q^2 \in [14.4, 25]$ GeV^2, showing the insensitivity on the number of KK modes in summation.

	$R_V = -2$		$R_V = 0$		$R_V = 2$		$R_V = 4$		$R_V = 6$	
R_f	5 KK level	20 KK level	5 KK level	20 KK level	5 KK level	20 KK level	5 KK level	20 KK level	5 KK level	20 KK level
−2	93.98	102.71	135.20	143.26	173.18	186.51	201.16	208.14	214.90	219.42
0	275.38	287.70	294.61	306.26	321.36	335.18	385.31	402.21	451.28	462.56
2	278.12	289.12	335.84	346.81	404.55	415.20	476.01	487.36	528.23	538.32
4	283.62	294.45	357.83	365.52	569.46	566.05	632.68	640.82	687.64	698.48
6	324.84	334.60	451.28	465.75	572.20	586.54	676.65	697.35	726.12	737.88

corresponding to different choices of BLT parameters. The numbers in the tables also indicate that our results are not very sensitive to the number of KK levels considered in the sum while calculating loop diagrams corresponding to different WCs.

In the left and right panels of Fig. 4, we present the region of parameter space which has been excluded by the currently measured experimental values of branching ratios of $B \to X_s \ell^+ \ell^-$ for two different q^2 regions, $[1, 6]$ GeV^2 and $[14.4, 25]$ GeV^2, respectively. In both of these panels, we have depicted contours corresponding to five different values of R_V in the $R_f - R^{-1}$ plane. The region under an individual curve (specified by a fixed value of R_V) has been excluded by comparing the experimentally measured branching ratio of $B \to X_s \ell^+ \ell^-$ to its theoretical prediction in the nmUED scenario. The curves represent the contours of constant branching ratios of $B \to X_s \ell^+ \ell^-$ corresponding to the 1σ upper limit of its experimentally measured value. One can understand the nature of these contour curves with the help of Figs. 2 and 3. With larger values of R^{-1}, KK masses increase, which leads to suppression in the decay width (and branching ratio). Hence, in order to overcome this suppression, one requires larger values of R_f and R_V. The larger values of the BLT parameter enhance the decay dynamics in two ways. First of all, these would diminish the KK masses. Secondly, larger values of R_f would increase the interaction strengths via the overlap integral I_1^n, whereas increasing values of R_V would increase interaction strengths via I_2^n.

To this end, we would like to mention that as far as the BLT parameters are concerned, there is no sharp contrast in the behavior of the decay branching ratio between two different regions of q^2. However, the lower limits of R^{-1} which we have obtained from our present analysis are slightly different for two different regions of q^2. In the case of the low-q^2 region ($\in [1, 6]$ GeV^2), the lower limit is higher than that of the case in the high-q^2 region ($\in [14.4, 25]$ GeV^2). For example (considering only the five-KK-level sum), in the low-q^2 region if we set $R_V = 4$, $R_f = 2$, the lower limit on R^{-1} is 536.38 GeV, while for the same set of BLT parameters R^{-1} is 476.01 GeV for the high-q^2 region. This feature is true for all combinations of BLT parameters. This feature indicates that, in the second case, the masses of the KK particles which are involved in the loop diagrams are relatively lighter with respect to the first case. This behavior is quite expected, because in the second case the phase space

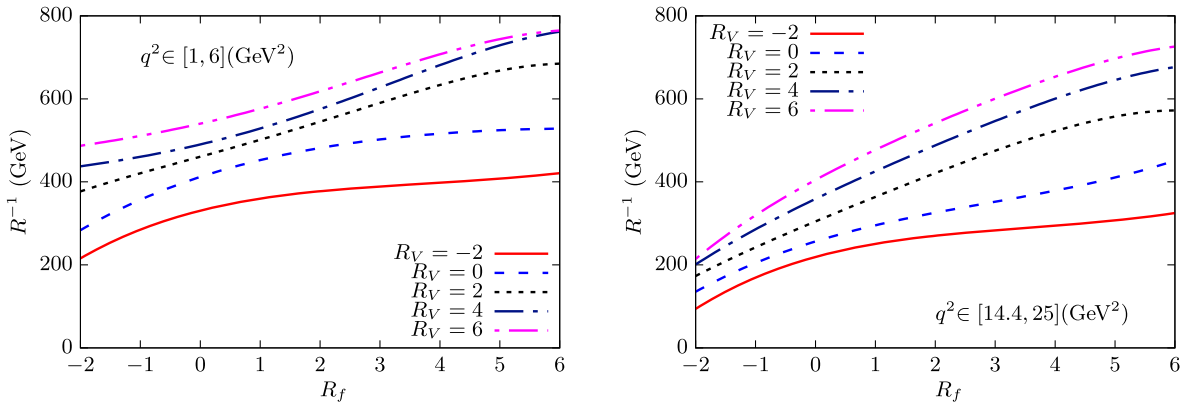

FIG. 4. Left and right panels represent the exclusion contours obtained from the branching ratio of $B \to X_s \ell^+ \ell^-$ decay in the $R_f - R^{-1}$ plane for low and high dilepton mass-squared regions, respectively, for five different choices of R_V. These exclusion curves have been drawn with the values of the lower limit of R^{-1} while we sum the contributions up to five KK levels in different loop functions required for the calculation of WCs. The area below a particular curve (fixed R_V) has been excluded by the experimental value of the branching ratio with a 1σ error bar.

suppression is larger with respect to the first one; hence, to compensate for this suppression, one requires relatively lighter mass particles which are involved in the loop diagrams needed for the calculation of different WCs.

Revisiting the lower limit on R^{-1} obtained from $B \to X_s \ell^+ \ell^-$ in the UED scenario.—Before we proceed any further, we would like to revisit the lower limit on R^{-1} obtained from our analysis in the UED scenario considering the current experimental results of the branching ratio of $B \to X_s \ell^+ \ell^-$. We can obtain the UED results from our analysis in the limit when both the BLT parameters vanish, i.e., for $R_V = R_f = 0$. In this limit, the KK mass for the nth KK level simply becomes nR^{-1}. Moreover, the overlap integrals I_1^n and I_2^n become unity. Hence, under this circumstance, the functions $D_n(x_t, x_{f^{(n)}}, x_{V^{(n)}})$ and $E_n(x_t, x_{f^{(n)}}, x_{V^{(n)}})$ given in Eqs. (38) and (39) would transform themselves into their UED forms. We have explicitly checked that in this vanishing BLT limit the expressions of the functions $D_n(x_t, x_{f^{(n)}}, x_{V^{(n)}})$ and $E_n(x_t, x_{f^{(n)}}, x_{V^{(n)}})$ are identical with the forms given in Ref. [61].[14] Under the same vanishing BLT limit condition, similar transformation is also applicable for other functions (e.g., C_n, Y_n, D'_n, and E'_n, which have been calculated in our previous articles [7,8]) required for the present calculations. Now, from our present analysis we can readily derive the lower limit on R^{-1} from Tables II and III. That is, for $R_V = R_f = 0$, the value of the lower limit on R^{-1} for $q^2 \in [1, 6]$ GeV^2 is 451.27 GeV, whereas for $q^2 \in [14.4, 25]$ GeV^2, the value changes to 294.61 GeV. It is needless to say that these results are not very strong but almost consistent with those values that are obtained from previous analyses in the UED scenario. For example, $(g-2)_\mu$ [80], ρ parameters [81], FCNC process [61,82–84], $Zb\bar{b}$ [56,85], and electroweak observables [86–88] put a lower bound of about 300–600 GeV on R^{-1}. On the other hand, from the projected trilepton signal at the 8 TeV LHC, one can derive a lower limit on R^{-1} up to 1.2 TeV [89–91]. At this point, it is worth mentioning that the values of the lower limit on R^{-1} obtained from the above mentioned analyses (for a minimal version of the UED scenario) have already been ruled out by the LHC data. The reason is that the recent analyses including LHC data exclude R^{-1} up to 1.4 TeV [92–95].

2. Forward-backward asymmetry

Finally, in Figs. 5 and 6, we have shown the forward-backward asymmetry [actually the global forward-backward asymmetry defined in Eq. (47)] for the decay $B \to X_s \ell^+ \ell^-$ for two q^2 regions, $[1, 6]$ GeV^2 and $[14.4, 25]$ GeV^2, respectively. In each figure, there are five panels corresponding to five different values of R_V. In each panel, we have depicted the variation of forward-backward asymmetry with respect to R^{-1} for five different values of R_f. Unlike the decay branching ratio, the behavior of forward-backward asymmetry has been significantly affected by the two different regions of q^2. For example, in the high-q^2 region, this asymmetry is always positive for the entire range of given R^{-1} for every combination of BLT parameters, whereas for the low-q^2 region, the sign (either positive or negative) of this asymmetry is crucially dependent on the BLT parameters for the lower values of R^{-1}, although it is always negative for higher values of R^{-1}. We have already mentioned that, in the present decay process among all the WCs, only $\tilde{C}_{10}$ is moderately enhanced by NP effects. Furthermore, this coefficient is independent of q^2 but depends only on the parameters of the NP scenario. Now, this coefficient has appeared with a factor proportional to $\frac{q^2}{m_b^2}$ both in the numerator as well as in the denominator of the definition of global forward-backward asymmetry. Hence, depending on the value of q^2, the factor $\frac{q^2}{m_b^2}$ could play a crucial role for the defined asymmetry.

In the case of the low-q^2 region, apart from the factor of $\frac{q^2}{m_b^2}$, some of the WCs could control the behavior of forward-backward asymmetry for the lower values of R^{-1}. Since in this situation the masses of KK modes are not very high, forward-backward asymmetry has been hallmarked by the characteristics of different WCs. Now, in every panel specified by a fixed value of R_V, we observe that the asymmetry always shows monotonically decreasing behavior for negative values of R_f. We have earlier mentioned that for negative values of R_f, the KK mass is high; therefore, the loop functions are suppressed, which in turn decreases the asymmetry. On the other hand, when R_f changes to the positive side, leading to relatively smaller values of KK mass, then the loop functions are enhanced so that the WCs are increased, and consequently the forward-backward asymmetry shows increasing behavior. Then, with the increasing values of R^{-1}, this asymmetry decreases. Moreover, the same argument is also applicable for the R_V, because, if we look at the all panels, then we can readily infer that the above mentioned effects due to R_f are slightly magnified by increasing values of R_V. At this point, we would like to point out that using this asymmetry, we can maximally achieve the lower limit on R^{-1} up to $\simeq$600 GeV. This limit can be obtained by comparing the theoretically estimated value of forward-backward asymmetry in the present nmUED model with the 1σ lower bound of the corresponding experimental data. However, this value is not in agreement with the one that we have obtained from the branching ratio. On the other hand, for the high-q^2 region, the factor $\frac{q^2}{m_b^2}$ is highly dominating in nature. Therefore, unlike very low values of R^{-1}, the WCs will not get any scope to control the characteristics of the forward-backward asymmetry. As a result, after a certain

[14]The authors of Ref. [61] have not considered any radiative corrections to the KK masses in their analysis. Consequently, the KK mass at the nth KK-level is nR^{-1}.

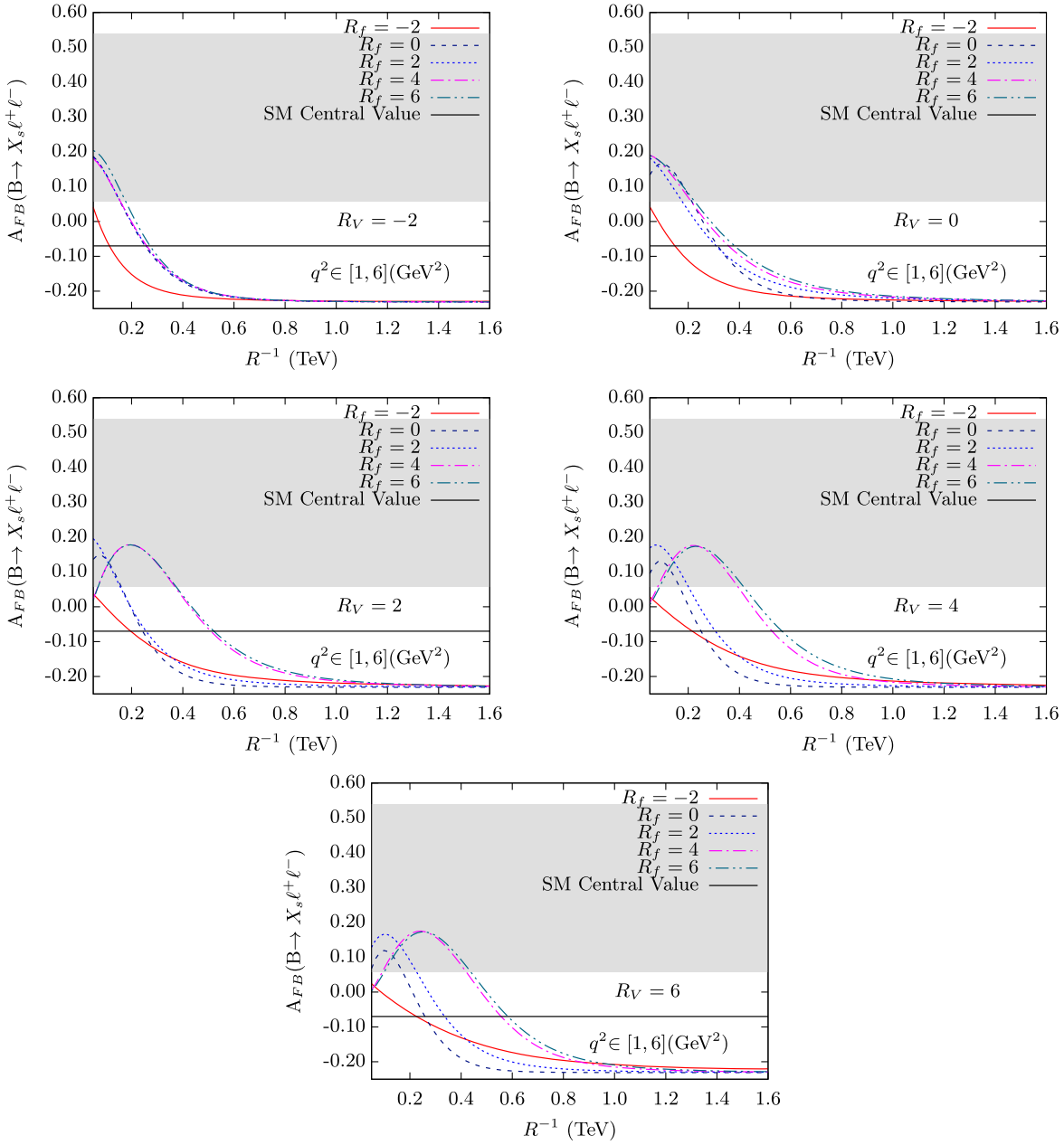

FIG. 5. Variation of the forward-backward asymmetry of $B \to X_s \ell^+ \ell^-$ with R^{-1} (TeV) for various values of $R_f (= r_f/R)$. The five panels represent different values of $R_V (= r_V/R)$. We sum the contributions up to five KK levels in different loop functions while calculating WCs. The horizontal gray band depicts the 1σ allowed range of experimental values of the forward-backward asymmetry for $q^2 \in [1, 6]$ GeV^2.

value of R^{-1}, both the numerator and the denominator of forward-backward asymmetry are totally affected by the same way by the factor $\frac{q^2}{m_b^2}$. Hence, the asymmetry practically becomes independent of R^{-1}. This is clearly evident from the plots, where this asymmetry is almost parallel to the R^{-1}. Depending on the values of the BLT parameters, the saturation behavior starts from different values of R^{-1}. However, it is also evident from the different panels of Fig. 6 that even for different combinations of BLT parameters, the threshold points (basically the value of R^{-1}) of this saturation behavior are not very distinct from each other.

3. Possible bounds on the nmUED scenario with upcoming measurements by the Belle II for the $B \to X_s \ell^+ \ell^-$ observables

In the near future, we will have new measurements by the Belle II experiment for the $B \to X_s \ell^+ \ell^-$ observables.

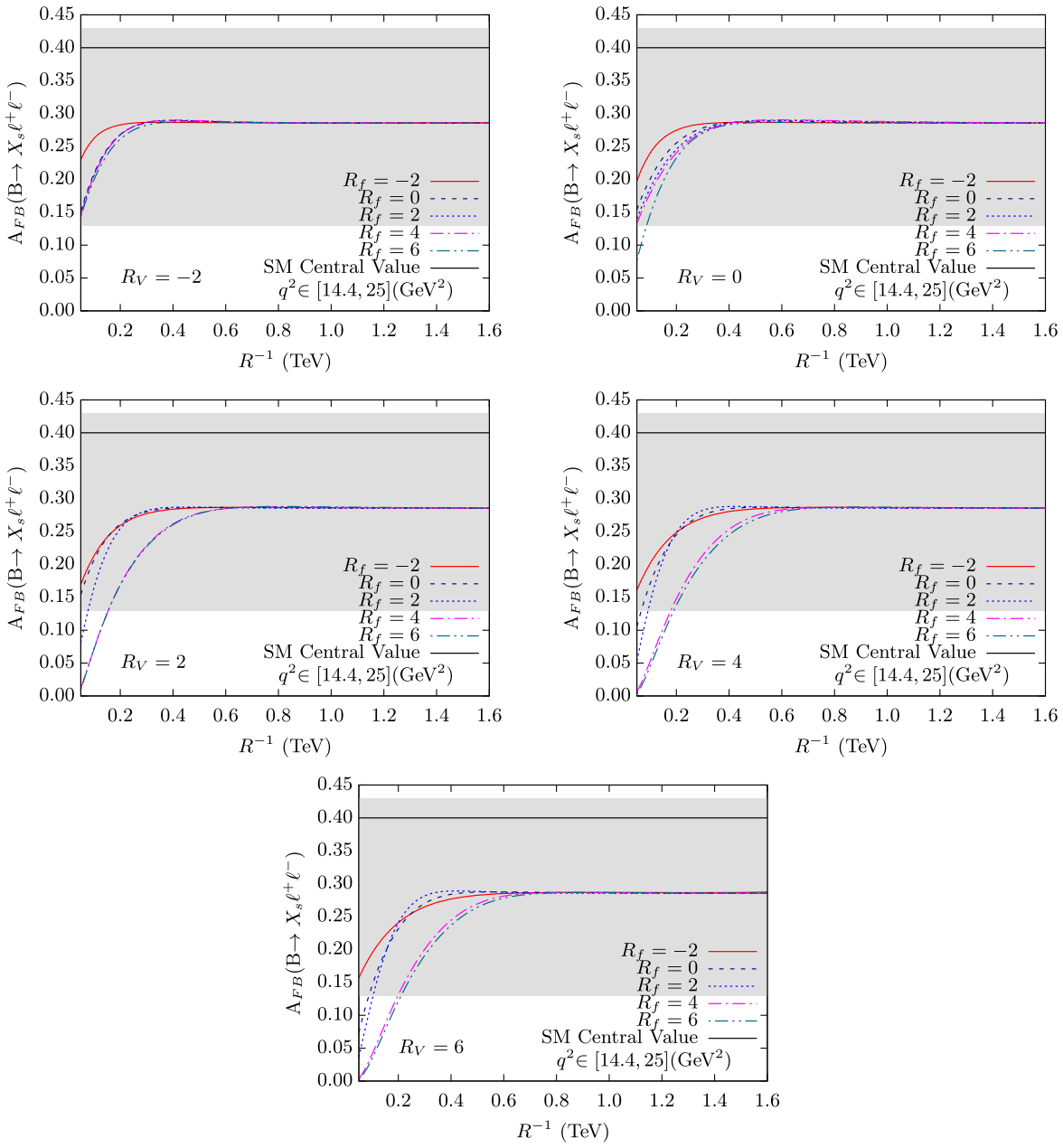

FIG. 6. Variation of the forward-backward asymmetry of $B \to X_s \ell^+ \ell^-$ with R^{-1} (TeV) for various values of $R_f (= r_f/R)$. The five panels represent different values of $R_V (= r_V/R)$. We sum the contributions up to five KK levels in different loop functions while calculating WCs. The horizontal gray band depicts the 1σ allowed range of experimental value of the forward-backward asymmetry for $q^2 \in [14.4, 25]$ GeV^2.

Therefore, at this stage it would be very relevant to discuss the possible bounds on the parameter space of the nmUED scenario in light of upcoming measurements by the Belle II experiment for the $B \to X_s \ell^+ \ell^-$ observables. Belle II can significantly improve the present situation with its 2-orders-of-magnitude larger data sample. Consequently, we can expect the reduction of systematic uncertainties for the various observables. In order to check the possible bounds on the parameter space of the nmUED scenario in the context of upcoming measurements by Belle II for the $B \to X_s \ell^+ \ell^-$ decay observables, we follow the prescription given in Refs. [15,96]. According to this prescription, the bounds can be implemented via the ratios R_9 and R_{10} under the assumption of no NP contributions to the electromagnetic and chromomagnetic dipole operators (i.e., $R_{7,8} = 1$), where the ratios are defined as $R_i = \frac{C_i}{C_i^{\text{SM}}}$ (C_is are different WCs, with $i = 7$, 8, 9, 10). In Fig. 4 of Ref. [15] (in all three panels), we can find a tiny area in the $R_9 - R_{10}$ plane that could be reached by upcoming results of the Belle II experiment. For all

cases within this tiny area, the values of both R_9 and R_{10} are very much close to unity. In other words, this fact indicates that the deviation between NP and SM predictions is very small. We translate this fact (using the lower panel of Fig. 4 of Ref. [15]) in the nmUED scenario in terms of the ratios R_9 and R_{10} from which we have obtained the bounds on the model parameters from the perspective of upcoming measurements by Belle II for the $B \to X_s \ell^+ \ell^-$ observables.

In the nmUED scenario, we have determined the values of the model parameters for which the ratios R_9 and R_{10} should be restricted within the tiny area in the $R_9 - R_{10}$ plane that could be reached by upcoming results of the Belle II experiment. The values of the lower limit of R^{-1} for different combinations of the BLT parameters R_f and R_V have been slightly shifted to higher values with respect to those which we have obtained from our main analysis in this article. For example, when $R_V = 2$ and $R_f = 4$, the lower limit on R^{-1} is 680.27 GeV, while this limit changes to 772.81 GeV for $R_V = 6$ and $R_f = 6$. This behavior is true for all combinations of BLT parameters. Here, we would like to mention that these values are obtained when we consider the sum up to five KK levels. This kind of result implies that the deviation between the SM expectation and the upcoming measurement by Belle II for the $B \to X_s \ell^+ \ell^-$ decay observables will be decreasing in nature. Consequently, the role of NP is expected to be more restricted for the $B \to X_s \ell^+ \ell^-$ decay observables. Therefore, one can constrain any NP model more precisely using the upcoming measurement by Belle II for the $B \to X_s \ell^+ \ell^-$ decay observables. Moreover, the tendency of increasing the lower limit of R^{-1} indicates that the NP model (in our case, the nmUED scenario) approaches the direction of the decoupling limit. As we have already mentioned, in a scenario like nmUED, where the masses of KK-excited states (NP particles in the present case) are essentially characterized by R^{-1}; therefore, with increasing values of R^{-1}, the masses of KK-excited states are increased. Consequently, the effects of these KK-excited states will be decreased.

V. SUMMARY AND CONCLUSION

In view of the findings of new physics effects, we have estimated the contributions of KK excitations to the decay of $B \to X_s \ell^+ \ell^-$ in a $(4+1)$-dimensional nonminimal universal extra dimensional scenario which is allowed to propagate all Standard Model particles. This specific scenario is characterized by different boundary-localized terms (kinetic, Yukawa, etc.). Actually, in the five-dimensional universal extra dimensional scenario, the unknown radiative corrections to the masses and couplings are parametrized by the strength of these boundary-localized terms. Hence, in the presence of these terms, the KK mass spectra as well as the interaction strengths among the various KK excitations are transformed in a nontrivial manner in the four-dimensional effective theory with respect to the minimal version of the universal extra dimensional scenario. In the present article, we have used two different categories of BLT parameters. For example, strengths for the boundary terms of fermions and Yukawa interactions are represented by r_f, while r_V represents the strengths of boundary terms for the gauge as well as Higgs sectors. We have examined the effects of these BLT parameters on the $B \to X_s \ell^+ \ell^-$ decay process.

The effective Hamiltonian for the decay process $B \to X_s \ell^+ \ell^-$ is characterized by several Wilson coefficients C_7, C_9, and C_{10}. In the nonminimal universal extra dimensional scenario, the coefficients C_7 and C_{10} have already been calculated in our previous articles. However, for the first time, we have calculated the coefficient C_9 in the nonminimal universal extra dimensional scenario using the relevant Feynman (penguin) diagrams shown in Fig. 1. With these several Wilson coefficients, we have computed the coefficients of electroweak dipole operators for photons and gluons for the first time in the nonminimal universal extra dimensional scenario. Applying the advantage of the Glashow Iliopoulos Maiani (GIM) mechanism, we have included contributions from all three generations of quarks in our analysis. We evaluated the total contribution that is obtained from the penguin diagrams and then added it with the corresponding Standard Model counterpart. Considering a recent analysis relating the stability on the Higgs boson mass and cutoff of a universal extra dimensional scenario [76], we have considered the summation up to five KK levels in our calculation. Furthermore, we have incorporated next-to-leading QCD corrections in our analysis.

For the present decay process, in order to maintain perturbativity, one has to impose an appropriate choice of kinematic cuts to eliminate $c\bar{c}$ resonances which show large peaks in the dilepton invariant mass spectrum. Consequently, this gives two distinct perturbative dilepton invariant mass-squared regions, called the low dilepton mass-squared region with $1\ \text{GeV}^2 < q^2 < 6\ \text{GeV}^2$, and also the high dilepton mass-squared region with $q^2 > 14.4\ \text{GeV}^2$. In these two regions, experimental data for the branching ratio as well as forward-backward asymmetry are available for the decay $B \to X_s \ell^+ \ell^-$. However, there exists only a narrow window between the Standard Model prediction and the experimental data for both the regions and for both quantities (branching ratio and forward-backward asymmetry). Comparing our theoretical predictions with the corresponding experimental data (with a 1σ error bar), we have constrained the parameter space of the present version of the nonminimal universal extra dimensional scenario. During our analysis, we have used the branching ratios of some rare decay processes such as $B_s \to \mu^+ \mu^-$ and $B \to X_s \gamma$, as well as electroweak precision data, as constraints.

As we have already mentioned, from our analysis we can also reproduce the results of the minimal version of the

universal extra dimensional scenario by setting the BLT parameters to zero (i.e., $R_f = R_V = 0$). Hence, from our analysis we have revisited the lower limit on R^{-1} in the framework of the minimal universal extra dimensional scenario. Using the experimental data of the branching ratio, the lower limit becomes 451.27 (294.61) GeV for the low (high) q^2 region. Definitely, these results are comparable with the values that are obtained from the earlier analysis existing in the literature, although they are ruled out by recent collider analysis at the LHC. However, by the virtue of the presence of different nonzero BLT parameters, we can improve the results of the lower limit on R^{-1} in the present version of the nonminimal universal extra dimensional scenario. For example, for $R_V = 6$ and $R_f = 6$, using the branching ratio, we obtain the lower limit of $R^{-1} \geq 760$ GeV for the low-q^2 region, while the limit changes to $R^{-1} \geq 720$ GeV for the high-q^2 region. Obviously, these results in the context of the nonminimal universal extra dimensional scenario are very promising, because they exclude a large portion of the parameter space of the present scenario. Also, the obtained lower limit on R^{-1} is in the same ballpark as the limit obtained from previous analysis on $B_s \to \mu^+\mu^-$ [7] in the nonminimal universal extra dimensional scenario. Furthermore, from Fig. 4, it is clearly evident that the lower limits on R^{-1} are relatively more competitive for positive values of the BLT parameters rather than their negative values. Unfortunately, the limits which we have obtained on the parameter space (of the nonminimal universal extra dimensional scenario) using the forward-backward asymmetry of the decay $B \to X_s \ell^+ \ell^-$ are not so competitive.

Moreover, we have tried to determine the possible bounds on the model parameters of the nonminimal universal extra dimensional scenario with upcoming measurements by Belle II for the $B \to X_s \ell^+ \ell^-$ observables. We have found that, for all combinations of the BLT parameters R_f and R_V, the lower limit of R^{-1} has been slightly shifted to higher values with respect to the values which we have achieved from our main analysis in this article.

ACKNOWLEDGMENTS

The author is grateful to Anindya Datta for taking part in the initial stage and for many useful discussions. The author is very thankful to Andrzej J. Buras for useful suggestions. The author would also like to give thanks to Anirban Biswas for computational support.

APPENDIX A: SOME IMPORTANT FUNCTIONS AND WILSON COEFFICIENTS THAT ARE REQUIRED FOR THE CALCULATION OF $B \to X_s \ell^+ \ell^-$ IN nmUED

Functions [69]:

$$\omega\left(\frac{q^2}{m_b^2}\right) = -\frac{2}{9}\pi^2 - \frac{4}{3}\mathrm{Li}_2\left(\frac{q^2}{m_b^2}\right) - \frac{2}{3}\ln\left(\frac{q^2}{m_b^2}\right)\ln\left(1-\frac{q^2}{m_b^2}\right) - \frac{5+4\frac{q^2}{m_b^2}}{3(1+2\frac{q^2}{m_b^2})}\ln\left(1-\frac{q^2}{m_b^2}\right) - \frac{2\frac{q^2}{m_b^2}(1+\frac{q^2}{m_b^2})(1-2\frac{q^2}{m_b^2})}{3(1-\frac{q^2}{m_b^2})^2(1+2\frac{q^2}{m_b^2})}\ln\left(\frac{q^2}{m_b^2}\right) + \frac{5+9\frac{q^2}{m_b^2}-6(\frac{q^2}{m_b^2})^2}{6(1-\frac{q^2}{m_b^2})(1+2\frac{q^2}{m_b^2})} \tag{A1}$$

and

$$h\left(z,\frac{q^2}{m_b^2}\right) = \frac{8}{27} - \frac{8}{9}\ln\frac{m_b}{\mu} - \frac{8}{9}\ln z + \frac{16z^2m_b^2}{9q^2} - \frac{4}{9}\left(1+\frac{2z^2m_b^2}{q^2}\right)\sqrt{|1-\frac{4z^2m_b^2}{q^2}|}\begin{cases}\ln\left|\frac{\sqrt{1-\frac{4z^2m_b^2}{q^2}}+1}{\sqrt{1-\frac{4z^2m_b^2}{q^2}}-1}\right| - i\pi, & \text{if } \frac{4z^2m_b^2}{q^2} < 1 \\ 2\arctan\frac{1}{\sqrt{\frac{4z^2m_b^2}{q^2}-1}}, & \text{if } \frac{4z^2m_b^2}{q^2} > 1\end{cases} \tag{A2}$$

$$h\left(0,\frac{q^2}{m_b^2}\right) = \frac{8}{27} - \frac{8}{9}\ln\frac{m_b}{\mu} - \frac{4}{9}\ln\left(\frac{q^2}{m_b^2}\right) + \frac{4}{9}i\pi. \tag{A3}$$

Wilson coefficients: $C_1 \ldots C_6$ [71]:

$$C_1^{(0)}(M_W) = \frac{11}{2}\frac{\alpha_s(M_W)}{4\pi}, \tag{A4}$$

$$C_2^{(0)}(M_W) = 1 - \frac{11}{6}\frac{\alpha_s(M_W)}{4\pi}, \tag{A5}$$

$$C_3^{(0)}(M_W) = -\frac{1}{3}C_4^{(0)}(M_W) = -\frac{\alpha_s(M_W)}{24\pi} = \tilde{E}(x_t, r_f, r_V, R^{-1}), \tag{A6}$$

$$C_5^{(0)}(M_W) = -\frac{1}{3}C_6^{(0)}(M_W) = -\frac{\alpha_s(M_W)}{24\pi} = \tilde{E}(x_t, r_f, r_V, R^{-1}), \tag{A7}$$

where

$$\tilde{E}(x_t, r_f, r_V, R^{-1}) = E(x_t, r_f, r_V, R^{-1}) - \frac{2}{3}. \tag{A8}$$

C_7 [69]:

$$C_{7\gamma}^{(0)\text{eff}} = \eta^{\frac{16}{23}} C_{7\gamma}^{(0)}(M_W) + \frac{8}{3}(\eta^{\frac{14}{23}} - \eta^{\frac{16}{23}}) C_{8G}^{(0)}(M_W) + C_2^{(0)}(M_W)\sum_{i=1}^{8} h_i \eta^{a_i}, \tag{A9}$$

with

$$\eta = \frac{\alpha_s(M_W)}{\alpha_s(m_b)}, \qquad \alpha_s(m_b) = \frac{\alpha_s(M_Z)}{1 - \beta_0 \frac{\alpha_s(M_Z)}{2\pi}\ln(M_Z/m_b)}, \qquad \beta_0 = \frac{23}{3}, \tag{A10}$$

and

$$C_{7\gamma}^{(0)}(M_W) = -\frac{1}{2}D'(x_t, r_f, r_V, R^{-1}), \tag{A11}$$

$$C_{8G}^{(0)}(M_W) = -\frac{1}{2}E'(x_t, r_f, r_V, R^{-1}). \tag{A12}$$

The values of a_i, h_i, and $\bar{h}_i$ can be obtained from Ref. [61]. The functions $D'(x_t, r_f, r_V, R^{-1})$ and $E'(x_t, r_f, r_V, R^{-1})$ are the total (SM + nmUED) contributions at the LO as given in Ref. [8].

APPENDIX B: FEYNMAN RULES FOR $B \to X_s \ell^+ \ell^-$ IN nmUED

In this appendix, we have given the relevant Feynman rules for our calculations. All momenta and fields are assumed to be incoming. $\hat{A}$ represents the background photon field.

(1) $\hat{A}^\mu W^{\nu\pm} S^\mp$: $g_2 s_w M_{W^{(n)}} g_{\mu\nu} C$, where C is given in the following:

$$\begin{aligned} &\hat{A}^\mu W^{\nu(n)+} G^{(n)-}:\ C = 0,\\ &\hat{A}^\mu W^{\nu(n)-} G^{(n)+}:\ C = 0,\\ &\hat{A}^\mu W^{\nu(n)+} H^{(n)-}:\ C = 0,\\ &\hat{A}^\mu W^{\nu(n)-} H^{(n)+}:\ C = 0, \end{aligned} \tag{B1}$$

where g_2 represents the $SU(2)$ gauge coupling constant, while s_w denotes the sine of the Weinberg angle (θ_w).

(2) $\hat{A}^\mu S_1^\pm S_2^\mp$: $-ig_2 s_w (k_2 - k_1)_\mu C$, where C is given in the following:

$$\begin{aligned} &\hat{A}^\mu G^{(n)+} G^{(n)-}:\ C = 1,\\ &\hat{A}^\mu H^{(n)+} H^{(n)-}:\ C = 1,\\ &\hat{A}^\mu G^{(n)+} H^{(n)-}:\ C = 0,\\ &\hat{A}^\mu G^{(n)-} H^{(n)+}:\ C = 0, \end{aligned} \tag{B2}$$

where the scalar fields $S \equiv H, G$.

(3) $\hat{A}^\mu(k_1) W^{\nu+}(k_2) W^{\lambda-}(k_3)$:

$$ig_2 s_w [g_{\mu\nu}(k_2 - k_1 + k_3)_\lambda + g_{\mu\lambda}(k_1 - k_3 - k_2)_\nu + g_{\lambda\nu}(k_3 - k_2)_\mu]. \tag{B3}$$

(4) $\hat{A}^\mu \bar{f}_1 f_2$: $ig_2 s_w \gamma_\mu C$, where C is given in the following:

$$\begin{aligned} \hat{A}^\mu \bar{u}_i u_i:\ C &= \frac{2}{3},\\ \hat{A}^\mu \bar{T}_i^{1(n)} T_i^{1(n)}:\ C &= \frac{2}{3},\\ \hat{A}^\mu \bar{T}_i^{2(n)} T_i^{2(n)}:\ C &= \frac{2}{3},\\ \hat{A}^\mu \bar{T}_i^{1(n)} T_i^{2(n)}:\ C &= 0,\\ \hat{A}^\mu \bar{T}_i^{2(n)} T_i^{2(n)}:\ C &= 0. \end{aligned} \tag{B4}$$

(5) $G^\mu \bar{f}_1 f_2$: $ig_s T^a_{\alpha\beta} \gamma_\mu C$, where C is given in the following:

$$\begin{aligned} G^\mu \bar{u}_i u_i:\ C &= 1,\\ G^\mu \bar{T}_i^{1(n)} T_i^{1(n)}:\ C &= 1,\\ G^\mu \bar{T}_i^{2(n)} T_i^{2(n)}:\ C &= 1,\\ G^\mu \bar{T}_i^{1(n)} T_i^{2(n)}:\ C &= 0,\\ G^\mu \bar{T}_i^{2(n)} T_i^{2(n)}:\ C &= 0. \end{aligned} \tag{B5}$$

(6) $S^{\pm}\bar{f}_1 f_2 = \frac{g_2}{\sqrt{2}M_{W^{(n)}}}(P_L C_L + P_R C_R)$, where C_L and C_R are given in the following:

$$
\begin{aligned}
G^+\bar{u}_i d_j&:\begin{cases} C_L = -m_i V_{ij}, \\ C_R = m_j V_{ij}, \end{cases} & G^-\bar{d}_j u_i&:\begin{cases} C_L = -m_j V^*_{ij}, \\ C_R = m_i V^*_{ij}, \end{cases} \\
G^{(n)+}\bar{T}^{1(n)}_i d_j&:\begin{cases} C_L = -m^{(i)}_1 V_{ij}, \\ C_R = M^{(i,j)}_1 V_{ij}, \end{cases} & G^{(n)-}\bar{d}_j T^{1(n)}_i&:\begin{cases} C_L = -M^{(i,j)}_1 V^*_{ij}, \\ C_R = m^{(i)}_1 V^*_{ij}, \end{cases} \\
G^{(n)+}\bar{T}^{2(n)}_i d_j&:\begin{cases} C_L = m^{(i)}_2 V_{ij}, \\ C_R = -M^{(i,j)}_2 V_{ij}, \end{cases} & G^{(n)-}\bar{d}_j T^{2(n)}_i&:\begin{cases} C_L = M^{(i,j)}_2 V^*_{ij}, \\ C_R = -m^{(i)}_2 V^*_{ij}, \end{cases} \\
H^{(n)+}\bar{T}^{1(n)}_i d_j&:\begin{cases} C_L = -m^{(i)}_3 V_{ij}, \\ C_R = M^{(i,j)}_3 V_{ij}, \end{cases} & H^{(n)-}\bar{d}_j T^{1(n)}_i&:\begin{cases} C_L = -M^{(i,j)}_3 V^*_{ij}, \\ C_R = m^{(i)}_3 V^*_{ij}, \end{cases} \\
H^{(n)+}\bar{T}^{2(n)}_i d_j&:\begin{cases} C_L = m^{(i)}_4 V_{ij}, \\ C_R = -M^{(i,j)}_4 V_{ij}, \end{cases} & H^{(n)-}\bar{d}_j T^{2(n)}_i&:\begin{cases} C_L = M^{(i,j)}_4 V^*_{ij}, \\ C_R = -m^{(i)}_4 V^*_{ij}. \end{cases}
\end{aligned}
\tag{B6}
$$

(7) 7. $W^{\mu\pm}\bar{f}_1 f_2$: $\frac{ig_2}{\sqrt{2}}\gamma_\mu P_L C_L$, where C_L is given in the following:

$$
\begin{aligned}
W^{\mu+}\bar{u}_i d_j&: \quad C_L = V_{ij}, & W^{\mu-}\bar{d}_j u_i&: \quad C_L = V^*_{ij}, \\
W^{\mu(n)+}\bar{T}^{1(n)}_i d_j&: \quad C_L = I^n_1 c_{\rm in} V_{ij}, & W^{\mu(n)-}\bar{d}_j T^{1(n)}_i&: \quad C_L = I^n_1 c_{\rm in} V^*_{ij}, \\
W^{\mu(n)+}\bar{T}^{2(n)}_i d_j&: \quad C_L = -I^n_1 s_{\rm in} V_{ij}, & W^{\mu(n)-}\bar{d}_j T^{2(n)}_i&: \quad C_L = -I^n_1 s_{\rm in} V^*_{ij},
\end{aligned}
\tag{B7}
$$

where the fermion fields $f \equiv u, d, T^1_l, T^2_l$.

The mass parameters $m^{(i)}_x$ are given in the following [7]:

$$
\begin{aligned}
m^{(i)}_1 &= I^n_2 m_{V^{(n)}} c_{\rm in} + I^n_1 m_i s_{\rm in}, \\
m^{(i)}_2 &= -I^n_2 m_{V^{(n)}} s_{\rm in} + I^n_1 m_i c_{\rm in}, \\
m^{(i)}_3 &= -I^n_2 i M_W c_{\rm in} + I^n_1 i \frac{m_{V^{(n)}} m_i}{M_W} s_{\rm in}, \\
m^{(i)}_4 &= I^n_2 i M_W s_{\rm in} + I^n_1 i \frac{m_{V^{(n)}} m_i}{M_W} c_{\rm in},
\end{aligned}
\tag{B8}
$$

where m_i denotes the mass of the zero-mode *up-type* fermion and $c_{\rm in} = \cos(\alpha_{\rm in})$ and $s_{\rm in} = \sin(\alpha_{\rm in})$, with $\alpha_{\rm in}$ as defined earlier.

The mass parameters $M^{(i,j)}_x$ are given in the following [7]:

$$
\begin{aligned}
M^{(i,j)}_1 &= I^n_1 m_j c_{\rm in}, \\
M^{(i,j)}_2 &= I^n_1 m_j s_{\rm in}, \\
M^{(i,j)}_3 &= I^n_1 i \frac{m_{V^{(n)}} m_j}{M_W} c_{\rm in}, \\
M^{(i,j)}_4 &= I^n_1 i \frac{m_{V^{(n)}} m_j}{M_W} s_{\rm in},
\end{aligned}
\tag{B9}
$$

where m_j denotes the mass of the zero-mode *down-type* fermion.

In all the Feynman vertices, the factors I_1^n and I_2^n are represented as the overlap integrals given in the following [7]:

$$I_1^n = 2\sqrt{\frac{1+\frac{r_V}{\pi R}}{1+\frac{r_f}{\pi R}}}\left[\frac{1}{\sqrt{1+\frac{r_f^2 m_{f^{(n)}}^2}{4}+\frac{r_f}{\pi R}}}\right]\left[\frac{1}{\sqrt{1+\frac{r_V^2 m_{V^{(n)}}^2}{4}+\frac{r_V}{\pi R}}}\right]\frac{m_{V^{(n)}}^2}{(m_{V^{(n)}}^2 - m_{f^{(n)}}^2)}\frac{(r_f - r_V)}{\pi R}, \tag{B10}$$

$$I_2^n = 2\sqrt{\frac{1+\frac{r_V}{\pi R}}{1+\frac{r_f}{\pi R}}}\left[\frac{1}{\sqrt{1+\frac{r_f^2 m_{f^{(n)}}^2}{4}+\frac{r_f}{\pi R}}}\right]\left[\frac{1}{\sqrt{1+\frac{r_V^2 m_{V^{(n)}}^2}{4}+\frac{r_V}{\pi R}}}\right]\frac{m_{V^{(n)}} m_{f^{(n)}}}{(m_{V^{(n)}}^2 - m_{f^{(n)}}^2)}\frac{(r_f - r_V)}{\pi R}. \tag{B11}$$

[1] G. Aad *et al.* (ATLAS Collaboration), Observation of a new particle in the search for the Standard Model Higgs boson with the ATLAS detector at the LHC, Phys. Lett. B **716**, 1 (2012).

[2] S. Chatrchyan *et al.* (CMS Collaboration), Observation of a new boson at a mass of 125 GeV with the CMS experiment at the LHC, Phys. Lett. B **716**, 30 (2012).

[3] HFAG, Average of $\mathcal{R}(D)$ and $\mathcal{R}(D^*)$ for FPCP 2017, http://www.slac.stanford.edu/xorg/hflav/semi/fpcp17/RDRDs.html.

[4] R. Aaij *et al.* (LHCb Collaboration), Measurement of the Ratio of Branching Fractions $\mathcal{B}(B_c^+ \to J/\psi\tau^+\nu_\tau)/\mathcal{B}(B_c^+ \to J/\psi\mu^+\nu_\mu)$, Phys. Rev. Lett. **120**, 121801 (2018).

[5] R. Aaij *et al.* (LHCb Collaboration), Search for Lepton-Universality Violation in $B^+ \to K^+\ell^+\ell^-$ decays, Phys. Rev. Lett. **122**, 191801 (2019).

[6] R. Aaij *et al.* (LHCb Collaboration), Test of lepton universality with $B^0 \to K^{*0}\ell^+\ell^-$ decays, J. High Energy Phys. 08 (2017) 055.

[7] A. Datta and A. Shaw, Nonminimal universal extra dimensional model confronts $B_s \to \mu^+\mu^-$, Phys. Rev. D **93**, 055048 (2016).

[8] A. Datta and A. Shaw, Effects of non-minimal universal extra dimension on $B \to X_s\gamma$, Phys. Rev. D **95**, 015033 (2017).

[9] A. Biswas, A. Shaw, and S. K. Patra, $\mathcal{R}(D^{(*)})$ anomalies in light of a nonminimal universal extra dimension, Phys. Rev. D **97**, 035019 (2018).

[10] T. Hurth, Present status of inclusive rare B decays, Rev. Mod. Phys. **75**, 1159 (2003).

[11] M. Benzke, T. Hurth, and S. Turczyk, Subleading power factorization in $\bar{B} \to X_s\ell^+\ell^-$, J. High Energy Phys. 10 (2017) 031.

[12] T.-F. Feng, J.-L. Yang, H.-B. Zhang, S.-M. Zhao, and R.-F. Zhu, $B \to X_s l^+ l^-$ in the minimal gauged $(B-L)$ supersymmetry, Phys. Rev. D **94**, 115034 (2016).

[13] J. Kumar and D. London, New physics in $b \to se^+e^-$? Phys. Rev. D **99**, 073008 (2019).

[14] J. P. Lees *et al.* (*BABAR* Collaboration), Measurement of the $B \to X_s l^+ l^-$ Branching Fraction and Search for Direct *CP* Violation from a Sum of Exclusive Final States, Phys. Rev. Lett. **112**, 211802 (2014).

[15] T. Huber, T. Hurth, and E. Lunghi, Inclusive $\bar{B} \to X_s\ell^+\ell^-$: Complete angular analysis and a thorough study of collinear photons, J. High Energy Phys. 06 (2015) 176.

[16] Y. Sato *et al.* (Belle Collaboration), Measurement of the lepton forward-backward asymmetry in $B \to X_s\ell^+\ell^-$ decays with a sum of exclusive modes, Phys. Rev. D **93**, 032008 (2016).

[17] S. Fukae, C. S. Kim, T. Morozumi, and T. Yoshikawa, A model independent analysis of the rare B decay $B \to X_s l^+ l^-$, Phys. Rev. D **59**, 074013 (1999).

[18] A. Ali, E. Lunghi, C. Greub, and G. Hiller, Improved model independent analysis of semileptonic and radiative rare B decays, Phys. Rev. D **66**, 034002 (2002).

[19] E. Lunghi, A. Masiero, I. Scimemi, and L. Silvestrini, $B \to X_s\ell^+\ell^-$ decays in supersymmetry, Nucl. Phys. **B568**, 120 (2000).

[20] T. Appelquist, H.-C. Cheng, and B. A. Dobrescu, Bounds on universal extra dimensions, Phys. Rev. D **64**, 035002 (2001).

[21] G. Servant and T. M. P. Tait, Elastic scattering and direct detection of Kaluza-Klein dark matter, New J. Phys. **4**, 99 (2002).

[22] G. Servant and T. M. P. Tait, Is the lightest Kaluza-Klein particle a viable dark matter candidate?, Nucl. Phys. **B650**, 391 (2003).

[23] H.-C. Cheng, J. L. Feng, and K. T. Matchev, Kaluza-Klein Dark Matter, Phys. Rev. Lett. **89**, 211301 (2002).

[24] D. Majumdar, Detection rates for Kaluza-Klein dark matter, Phys. Rev. D **67**, 095010 (2003).

[25] F. Burnell and G. D. Kribs, The abundance of Kaluza-Klein dark matter with coannihilation, Phys. Rev. D **73**, 015001 (2006).

[26] K. Kong and K. T. Matchev, Precise calculation of the relic density of Kaluza-Klein dark matter in universal extra dimensions, J. High Energy Phys. 01 (2006) 038.

[27] M. Kakizaki, S. Matsumoto, and M. Senami, Relic abundance of dark matter in the minimal universal extra dimension model, Phys. Rev. D **74**, 023504 (2006).

[28] G. Belanger, M. Kakizaki, and A. Pukhov, Dark matter in UED: The role of the second KK level, J. Cosmol. Astropart. Phys. 02 (2011) 009.

[29] K. R. Dienes, E. Dudas, and T. Gherghetta, Extra space-time dimensions and unification, Phys. Lett. B **436**, 55 (1998).

[30] K. R. Dienes, E. Dudas, and T. Gherghetta, Grand unification at intermediate mass scales through extra dimensions, Nucl. Phys. **B537**, 47 (1999).

[31] G. Bhattacharyya, A. Datta, S. K. Majee, and A. Raychaudhuri, Power law blitzkrieg in universal extra dimension scenarios, Nucl. Phys. **B760**, 117 (2007).

[32] K. Hsieh, R. N. Mohapatra, and S. Nasri, Dark matter in universal extra dimension models: Kaluza-Klein photon and right-handed neutrino admixture, Phys. Rev. D **74**, 066004 (2006).

[33] Y. Fujimoto, K. Nishiwaki, M. Sakamoto, and R. Takahashi, Realization of lepton masses and mixing angles from point interactions in an extra dimension, J. High Energy Phys. 10 (2014) 191.

[34] P. R. Archer, The Fermion mass hierarchy in models with warped extra dimensions and a bulk Higgs, J. High Energy Phys. 09 (2012) 095.

[35] H. Georgi, A. K. Grant, and G. Hailu, Brane couplings from bulk loops, Phys. Lett. B **506**, 207 (2001).

[36] H.-C. Cheng, K. T. Matchev, and M. Schmaltz, Radiative corrections to Kaluza-Klein masses, Phys. Rev. D **66**, 036005 (2002).

[37] G. R. Dvali, G. Gabadadze, M. Kolanovic, and F. Nitti, The power of brane induced gravity, Phys. Rev. D **64**, 084004 (2001).

[38] M. Carena, T. M. P. Tait, and C. E. M. Wagner, Branes and orbifolds are opaque, Acta Phys. Pol. B **33**, 2355 (2002).

[39] F. del Aguila, M. Perez-Victoria, and J. Santiago, Bulk fields with general brane kinetic terms, J. High Energy Phys. 02 (2003) 051.

[40] F. del Aguila, M. Perez-Victoria, and J. Santiago, Some consequences of brane kinetic terms for bulk fermions, in 38th Rencontres de Moriond on Electroweak Interactions and Unified Theories Les Arcs, France, 2003 (2003), https://arxiv.org/abs/hep-ph/0305119.

[41] F. del Aguila, M. Perez-Victoria, and J. Santiago, Physics of brane kinetic terms, Acta Phys. Pol. B **34**, 5511 (2003).

[42] C. Schwinn, Higgsless fermion masses and unitarity, Phys. Rev. D **69**, 116005 (2004).

[43] T. Flacke, A. Menon, and D. J. Phalen, Non-minimal universal extra dimensions, Phys. Rev. D **79**, 056009 (2009).

[44] A. Datta, U. K. Dey, A. Shaw, and A. Raychaudhuri, Universal extra-dimensional models with boundary localized kinetic terms: Probing at the LHC, Phys. Rev. D **87**, 076002 (2013).

[45] T. Flacke, K. Kong, and S. C. Park, Phenomenology of universal extra dimensions with bulk-masses and brane-localized terms, J. High Energy Phys. 05 (2013) 111.

[46] T. Flacke, K. Kong, and S. C. Park, 126 GeV Higgs in next-to-minimal universal extra dimensions, Phys. Lett. B **728**, 262 (2014).

[47] J. Bonnevier, H. Melbeus, A. Merle, and T. Ohlsson, Monoenergetic Gamma-rays from non-minimal Kaluza-Klein dark matter annihilations, Phys. Rev. D **85**, 043524 (2012).

[48] A. Datta, U. K. Dey, A. Raychaudhuri, and A. Shaw, Boundary localized terms in universal extra-dimensional models through a dark matter perspective, Phys. Rev. D **88**, 016011 (2013).

[49] U. K. Dey and T. S. Ray, Constraining minimal and non-minimal universal extra dimension models with Higgs couplings, Phys. Rev. D **88**, 056016 (2013).

[50] A. Datta, K. Nishiwaki, and S. Niyogi, Non-minimal universal extra dimensions: The strongly interacting sector at the large hadron collider, J. High Energy Phys. 11 (2012) 154.

[51] A. Datta, K. Nishiwaki, and S. Niyogi, Non-minimal Universal extra dimensions with brane local terms: The top quark sector, J. High Energy Phys. 01 (2014) 104.

[52] A. Datta, A. Raychaudhuri, and A. Shaw, LHC limits on KK-parity non-conservation in the strong sector of universal extra-dimension models, Phys. Lett. B **730**, 42 (2014).

[53] A. Shaw, KK-parity non-conservation in UED confronts LHC data, Eur. Phys. J. C **75**, 33 (2015).

[54] A. Shaw, Status of exclusion limits of the KK-parity non-conserving resonance production with updated 13 TeV LHC, Acta Phys. Pol. B **49**, 1421 (2018).

[55] N. Ganguly and A. Datta, Exploring non minimal universal extra dimensional model at the LHC, J. High Energy Phys. 10 (2018) 072.

[56] T. Jha and A. Datta, $Z \to b\bar{b}$ in non-minimal universal extra dimensional model, J. High Energy Phys. 03 (2015) 012.

[57] S. Dasgupta, U. K. Dey, T. Jha, and T. S. Ray, Status of a flavor-maximal nonminimal universal extra dimension model, Phys. Rev. D **98**, 055006 (2018).

[58] U. K. Dey and T. Jha, Rare top decays in minimal and nonminimal universal extra dimension models, Phys. Rev. D **94**, 056011 (2016).

[59] C.-W. Chiang, U. K. Dey, and T. Jha, $t \to cg$ and $t \to cZ$ in universal extra dimensional models, Eur. Phys. J. Plus **134**, 210 (2019).

[60] T. Jha, Unitarity constraints on non-minimal universal extra dimensional Model, J. Phys. G **45**, 115002 (2018).

[61] A. J. Buras, A. Poschenrieder, M. Spranger, and A. Weiler, The impact of universal extra dimensions on $B \to X_s\gamma$, $B \to X_s$ gluon, $B \to X_s\mu^+\mu^-$, $K_L \to \pi^0 e^+ e^-$ and ϵ'/ϵ, Nucl. Phys. **B678**, 455 (2004).

[62] A. Datta and A. Shaw, A note on gauge-fixing in the electroweak sector of non-minimal UED, Mod. Phys. Lett. A **31**, 1650181 (2016).

[63] N. G. Deshpande and M. Nazerimonfared, Flavor changing electromagnetic vertex in a nonlinear R_ξ gauge, Nucl. Phys. **B213**, 390 (1983).

[64] B. Grinstein, M. J. Savage, and M. B. Wise, $B \to X_s e^+ e^-$ in the six quark model, Nucl. Phys. **B319**, 271 (1989).

[65] C. Bobeth, M. Misiak, and J. Urban, Photonic penguins at two loops and m_t dependence of $BR[B \to X_s l^+ l^-]$, Nucl. Phys. **B574**, 291 (2000).

[66] C. Bobeth, P. Gambino, M. Gorbahn, and U. Haisch, Complete NNLO QCD analysis of $\bar{B} \to X_s l^+ l^-$ and higher order electroweak effects, J. High Energy Phys. 04 (2004) 071.
[67] T. Huber, E. Lunghi, M. Misiak, and D. Wyler, Electromagnetic logarithms in $\bar{B} \to X_s l^+ l^-$, Nucl. Phys. **B740**, 105 (2006).
[68] M. Misiak, The $b \to s e^+ e^-$ and $b \to s\gamma$ decays with next-to-leading logarithmic QCD corrections, Nucl. Phys. **B393**, 23 (1993).
[69] A. J. Buras and M. Munz, Effective Hamiltonian for $B \to X_s e^+ e^-$ beyond leading logarithms in the NDR and HV schemes, Phys. Rev. D **52**, 186 (1995).
[70] T. Inami and C. S. Lim, Effects of superheavy quarks and leptons in low-energy weak processes $K_L \to \mu\bar{\mu}$, $K^+ \to \pi^+ \nu\bar{\nu}$ and $K^0 \leftrightarrow \overline{K^0}$, Prog. Theor. Phys. **65**, 297 (1981).
[71] A. J. Buras, M. E. Lautenbacher, M. Misiak, and M. Munz, Direct CP violation in $K_L \to \pi^0 e^+ e^-$ beyond leading logarithms, Nucl. Phys. **B423**, 349 (1994).
[72] N. Cabibbo and L. Maiani, The lifetime of charmed particles, Phys. Lett. **79B**, 109 (1978).
[73] C. S. Kim and A. D. Martin, On the determination of $V(ub)$ and $V(cb)$ from semileptonic B decays, Phys. Lett. B **225**, 186 (1989).
[74] A. Ali, T. Mannel, and T. Morozumi, Forward backward asymmetry of dilepton angular distribution in the decay $b \to s\ell^+\ell^-$, Phys. Lett. B **273**, 505 (1991).
[75] M. Tanabashi *et al.* (Particle Data Group), Review of particle physics, Phys. Rev. D **98**, 030001 (2018).
[76] A. Datta and S. Raychaudhuri, Vacuum stability constraints and LHC searches for a model with a universal extra dimension, Phys. Rev. D **87**, 035018 (2013).
[77] P. Dey and G. Bhattacharyya, A comparison of ultraviolet sensitivities in universal, nonuniversal, and split extra dimensional models, Phys. Rev. D **70**, 116012 (2004).
[78] M. Aaboud *et al.* (ATLAS Collaboration), Study of the rare decays of B_s^0 and B^0 mesons into muon pairs using data collected during 2015 and 2016 with the ATLAS detector, J. High Energy Phys. 04 (2019) 098.
[79] Y. Amhis *et al.* (HFLAV Collaboration), Averages of b-hadron, c-hadron, and τ-lepton properties as of summer 2016, Eur. Phys. J. C **77**, 895 (2017).
[80] P. Nath and M. Yamaguchi, Effects of Kaluza-Klein excitations on $(g-2)_\mu$, Phys. Rev. D **60**, 116006 (1999).
[81] T. Appelquist and H.-U. Yee, Universal extra dimensions and the Higgs boson mass, Phys. Rev. D **67**, 055002 (2003).
[82] A. J. Buras, M. Spranger, and A. Weiler, The impact of universal extra dimensions on the unitarity triangle and rare K and B decays, Nucl. Phys. **B660**, 225 (2003).
[83] K. Agashe, N. G. Deshpande, and G. H. Wu, Universal extra dimensions and $b \to s\gamma$, Phys. Lett. B **514**, 309 (2001).
[84] D. Chakraverty, K. Huitu, and A. Kundu, Effects of universal extra dimensions on $B_0 - \bar{B}_0$ mixing, Phys. Lett. B **558**, 173 (2003).
[85] J. F. Oliver, J. Papavassiliou, and A. Santamaria, Universal extra dimensions and $Z \to b\bar{b}$, Phys. Rev. D **67**, 056002 (2003).
[86] A. Strumia, Bounds on Kaluza-Klein excitations of the SM vector bosons from electroweak tests, Phys. Lett. B **466**, 107 (1999).
[87] T. G. Rizzo and J. D. Wells, Electroweak precision measurements and collider probes of the standard model with large extra dimensions, Phys. Rev. D **61**, 016007 (1999).
[88] C. D. Carone, Electroweak constraints on extended models with extra dimensions, Phys. Rev. D **61**, 015008 (1999).
[89] A. Belyaev, M. Brown, J. Moreno, and C. Papineau, Discovering minimal universal extra dimensions (MUED) at the LHC, J. High Energy Phys. 06 (2013) 080.
[90] T. Golling *et al.*, *Physics at a 100 TeV pp Collider: Beyond the Standard Model Phenomena*, CERN Yellow Report (CERN, Geneva, 2017), p. 441.
[91] Y. Gershtein *et al.*, Working group report: New particles, forces, and dimensions, in *Proceedings, 2013 Community Summer Study on the Future of U.S. Particle Physics: Snowmass on the Mississippi (CSS2013): Minneapolis, MN, USA, 2013* (2013), http://lss.fnal.gov/archive/2013/conf/fermilab-conf-13-584-t.pdf.
[92] D. Choudhury and K. Ghosh, Bounds on universal extra dimension from LHC run I and II data, Phys. Lett. B **763**, 155 (2016).
[93] J. Beuria, A. Datta, D. Debnath, and K. T. Matchev, LHC collider phenomenology of minimal universal extra dimensions, Comput. Phys. Commun. **226**, 187 (2018).
[94] S. Chakraborty, S. Niyogi, and K. Sridhar, Constraining compressed versions of MUED and MSSM using soft tracks at the LHC, J. High Energy Phys. 07 (2017) 105.
[95] N. Deutschmann, T. Flacke, and J. S. Kim, Current LHC constraints on minimal universal extra dimensions, Phys. Lett. B **771**, 515 (2017).
[96] W. Altmannshofer *et al.* (Belle II Collaboration), The Belle II physics book, arXiv:1808.10567.